Western Washington University
Western CEDAR

WWU Graduate School Collection | WWU Graduate and Undergraduate Scholarship

Summer 2016

Mapping Interactions Between the Type-VI Secretion System Effector tAE1 and Its Putative Substrates Using NMR Spectroscopy

Robert C. (Robert Corey) Henderson
Western Washington University, robert.c.henderson575@gmail.com

Follow this and additional works at: https://cedar.wwu.edu/wwuet

 Part of the Chemistry Commons

Recommended Citation

Henderson, Robert C. (Robert Corey), "Mapping Interactions Between the Type-VI Secretion System Effector tAE1 and Its Putative Substrates Using NMR Spectroscopy" (2016). *WWU Graduate School Collection*. 521.
https://cedar.wwu.edu/wwuet/521

This Masters Thesis is brought to you for free and open access by the WWU Graduate and Undergraduate Scholarship at Western CEDAR. It has been accepted for inclusion in WWU Graduate School Collection by an authorized administrator of Western CEDAR. For more information, please contact westerncedar@wwu.edu.

Mapping Interactions between the Type-VI Secretion System Effector Tae1 and its Putative Substrates Using NMR Spectroscopy

By

Robert Corey Henderson

Accepted in Partial Completion

Of the Requirements for the Degree

Master of Science

Kathleen L. Kitto, Dean of the Graduate School

ADVISORY COMMITTEE

Chair, Dr. Spencer Anthony-Cahill

Dr. P. Clint Spiegel

Dr. Serge Smirnov

MASTER'S THESIS

In presenting this thesis in partial fulfillment of the requirements for a master's degree at Western Washington University, I grant to Western Washington University the non-exclusive royalty-free right to archive, reproduce, distribute, and display the thesis in any and all forms, including electronic format, via any digital library mechanisms maintained by WWU.

I represent and warrant this is my original work, and does not infringe or violate any rights of others. I warrant that I have obtained written permissions from the owner of any third party copyrighted material included in these files.

I acknowledge that I retain ownership rights to the copyright of this work, including but not limited to the right to use all or part of this work in future works, such as articles or books.

Library users are granted permission for individual, research and non-commercial reproduction of this work for educational purposes only. Any further digital posting of this document requires specific permission from the author.

Any copying or publication of this thesis for commercial purposes, or for financial gain, is not allowed without my written permission.

Signature: R. Corey Henderson

Date: 07/20/2016

Mapping Interactions between the Type-VI Secretion System Effector Tae1 and its Putative Substrates Using NMR Spectroscopy

A Thesis

Presented To

The Faculty of

Western Washington University

In Partial Fulfillment

Of the Requirements for the Degree

Master of Science

By

Robert Corey Henderson

06/29/2016

Abstract

Tae1 is an amidase produced by gram negative Pseudomonas bacteria that attacks the peptidoglycan layer in the cell walls of neighboring bacteria after secretion through the Type VI secretion system (T6S). The goal of our work is mapping interactions between the type-VI-secretion system effector Tae1 and its putative substrates using nuclear magnetic resonance (NMR) spectroscopy. Tae1 is amenable to NMR in that we are able to collect spectra with resolved, well defined peaks that can be assigned, thereby providing valuable structural information. We have assigned 89.2% of backbone atoms and 87.4% of sidechain atoms. Assignment of Tae1 was performed with ^{15}N-HSQC, HNCA, HNCOCA, HNCACB, CBCACONH, HCCH COSY, HCCH TOCSY, and HCONH TOCSY experiments. Peptidoglycan binding experiments were performed using via ^{15}N-HSQC to monitor backbone residues and ^{13}C-HSQC to monitor sidechain residues. So far, these experiments have not revealed the molecular mechanism by which Tae1 recognizes its specific substrate; however, with the very high degree of assignment achieved in NMR experimentation, once a minimal binding fragment has been isolated determination of the binding mechanism will be easily achieved.

Acknowledgments

I would like to express my sincere gratitude to the following individuals:

My advisor, Dr. Spencer Anthony-Cahill without whom I don't know where I would be. His knowledge and passion for biochemistry have encouraged and inspired me to push myself further than I thought possible.

My committee members, Dr. P. Clint Spiegel, and Dr. Serge Smirnov for their availability and support.

Dr. Peter Brzovic for his training and support for NMR.

Dr. Seemay Chou for her immense efforts, incredible patience, and time donated to this project.

Past and present group members for creating a positive and successful environment.

My wonderfully supportive wife Laura, who has been with me at every step; and lastly my family who have given me so much encouragement along the way.

Table of Contents

List of Figures

With multi-drug resistant bacteria becoming more and more prevalent, we can no longer rely on well-established antibiotics to treat life-threatening bacterial infections. As pathogenic bacteria have become resistant to humanity's primary defense against them, a detailed understanding of resistance in pathogenic bacteria is an imperative. Among the most important research to be done currently is the development of new antibiotics so that resistant infections can be treated successfully (Taneja *et al.* 2016). Research regarding potential targets for novel antibiotics is focused on conserved structures unique to bacteria that are necessary for their survival. One of the most conserved and critical structures ubiquitous throughout the bacterial kingdom is the bacterial cell wall (Kuhner *et al.* 2014).

The bacterial cellular envelope is composed of the plasma membrane and the cell wall; it is the bacterium's first line of defense against threats it encounters in its environment. The bacterial envelope was viewed until the 1950's as a simple self-assembling semipermeable sack around the cell (Silhavy *et al.* 2010). We now know that the bacterial cellular envelope is a complex and varied structure that requires a significant investment of energy to assemble and maintain (Brown *et al.* 2013).

The cellular envelope must protect the bacterium from its hostile and often rapidly changing environment, while still allowing selective transport of nutrients into the cytosol (Silhavy *et al.* 2010). Investigation into the bacterial cellular envelope led to the development of the famous Gram staining technique (Taneja *et al.* 2016). There are two major classes of bacterial cellular envelopes characterized by the Gram stain: gram

positive, and gram negative (Figure 1). Gram positive bacteria such as *S. aureus* have an inner membrane surrounded by a thick layer of peptidoglycan (PG) composing the bacterial cell wall. In contrast, gram negative bacteria, such as *E. coli*, have a much thinner peptidoglycan cell wall but a second protective membrane outside of the peptidoglycan layer (Gan *et al.* 2008). The entire PG layer with the proteins and remaining cellular components removed is known as the bacterial sacculus. The sacculus is a gigadalton-large, highly dynamic, heterogeneous structure, which has proven difficult to characterize structurally (Schanda *et al.* 2014). While the composition of the peptidoglycan wall is well-characterized through electron cryotomography and atomic-force microscopy, protein-peptidoglycan, and peptidoglycan interaction with antibiotics have been difficult to elucidate (Schanda *et al.* 2014).

Figure 1: Simplified structure of Gram +/Gram – cells. Image Available at: http://www.sigmaaldrich.com/technical-documents/articles/biology/glycobiology/peptidoglycans.html.

The peptidoglycan cell wall is the prokaryotic cell's molecular coat of armor. As shown in Figure 2, it is a rigid structure with a backbone composed of repeating alternating units of the monosaccharides N-acetyl glucosamine (GlcNAc) and N-acetyl muramic acid (MurNAc) with a network of cross-linked peptides extending from the glycan backbone (Gan *et al.* 2008). Positions of the crosslinks can vary among bacterial

species but in general are conserved within a particular species (Silhavy *et al.* 2010). The rigid peptidoglycan cell wall makes up a single macromolecule surrounding the cell (Romaniuk *et al.* 2015). The cell wall provides structural support for the cell, creates the characteristic shapes of many bacteria, and confers resistance to turgor pressure (Chou *et al.* 2012). That prokaryotic cells do not lyse in a dilute solution such as distilled water is mediated, in the greatest part, by the peptidoglycan cell wall (Silhavy *et al.* 2010).

Molecular structure of peptidoglycan

Figure 2: Structure of peptidoglycan. Image modified from American Society for Microbiology. Original available at: http://cmr.asm.org/content/18/3/521/F2.expansion.html. Accessed October 18, 2014.

As the cell wall is rigid, a cell must break down and reform the peptidoglycan for growth and division. The maintenance of the peptidoglycan cell wall is an energy intensive process. Formation is a multistep mechanism where pentapeptide precursors are formed within the cytosol, and must be exported to the outside of the cell (Gan *et al.* 2008). These precursors are generally excreted at a small inlet of the cell wall known as the septum (Typas *et al.* 2012). Once they are excreted they are covalently bound to the GlcNAc/MurNAc by specific enzymes. Maintenance, in terms of peptidoglycan breakdown is a process which is carried out by a host of "housekeeping enzymes" (Chou *et al.* 2012). Among these housekeeping enzymes are amidases which catalyze the breakdown of peptidoglycan, and penicillin binding proteins which are necessary for catalyzing the cross-linking of new peptidoglycan (Chou *et al.* 2012).

Because PG is only observed in prokaryotes it makes a desirable target with reduced risk to eukaryotic cells. Many of modern medicine's frontline antibiotics already target PG (Kuner *et al.* 2014). For instance, penicillin targets one of the proteins responsible for the maintenance of the peptidoglycan layer (Otero *et al.* 2013). Penicillin and its derivatives like methicillin are known as β-lactam antibiotics due to their bicyclic ring structure, as shown in Figure 3, and inhibit one of the proteins which reforms the peptidoglycan known as penicillin binding protein (Otero *et al.* 2013). When the cell can no longer maintain its cell wall it will lyse and die.

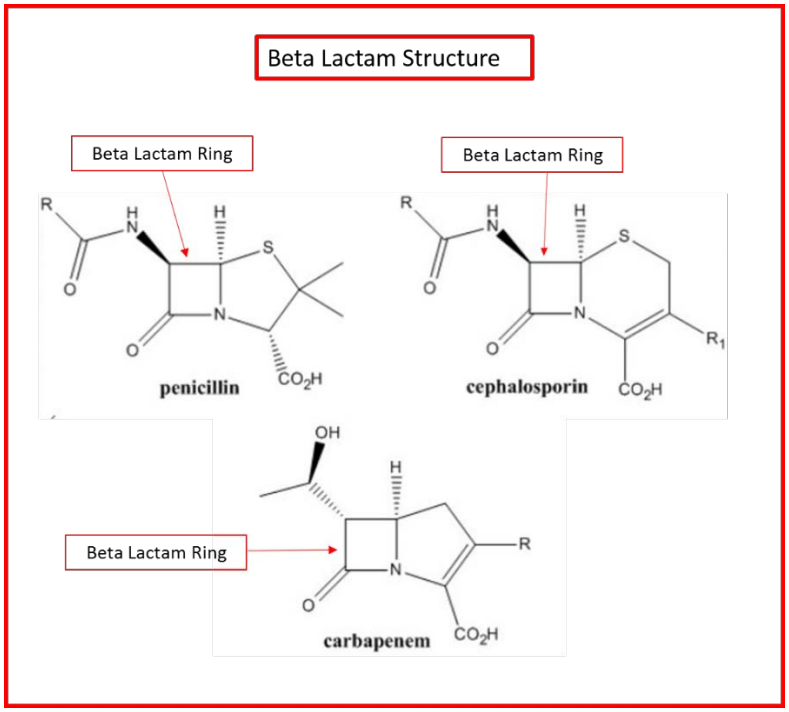

Figure 3: Structures of Beta lactam antibiotics

Within the last 60 years the detailed analysis of the structure of PG has been attempted by various methods (Kühner *et al.* 2014). Because of peptidoglycan's immense size and inherent flexibility, PG does not crystallize for X-ray diffraction

imaging methods, and is only amenable to NMR solution-state experiments with muropeptide fragments or solid-state NMR investigation (Desmarais *et al.* 2014; Schanda *et al.* 2014). To date the most effective methods of probing PG structure have been the application of liquid chromatography to analyze muropeptide fragments, and electron microscopy of whole sacculi (Kühner *et al.* 2014). These techniques are limited to providing information on bulk PG structure, and crosslinking of the peptides. They cannot provide atomic-level detail to protein/PG interactions (Schanda *et al.* 2014).

High pressure liquid chromatography and ultra-pressure liquid chromatography (HPLC/UPLC) methods carried out on muropeptides has proven useful in characterizing the structure of peptidoglycan crosslinks (Desmarais *et al.* 2014). Muropeptides are fragments of peptidoglycan consisting of peptides of various lengths bound to N-acetylmuramic acid generated from enzymatic digestion of the PG into disaccharides (Kühner *et al.* 2014). As they are a substantially smaller size than the intact bacterial sacculi they can also be utilized in experimental investigations of substrate binding to PG-modifying enzymes (Kuhner *et al.* 2014).

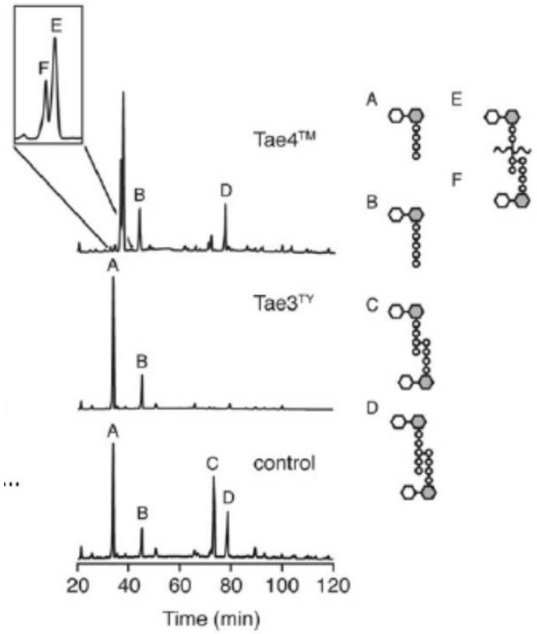

Figure 4: HPLC analysis of muropeptide fragments after digestion with Tae4 and Tae3 as well as a control displaying all possible fragments. See "Figure 4a" Russell et al., 2012, "A Widespread Bacterial Type VI Secretion Effector Superfamily Identified Using a Heuristic Approach;" Cell Host and Microbe 11: 538–549.

Substrate cleavage specificity studies are performed by treating intact bacterial sacculi with the enzyme of interest, and subsequently treating the resulting reaction mixture with an enzyme to digest (and thereby remove) the glycan strand. The remaining peptide fragments are then analyzed by HPLC/UPLC (Figure 4) to elucidate the site at which the enzyme of study is cleaving the PG (Kuhner *et al.* 2014). If no PG cleavage is performed by the enzyme of interest one would observe PG fragments of the same distribution as simply treating with lysozyme or muramidase. Furthermore, if the PG degrading enzyme of interest is promiscuous in its cleavage one would observe a broad distribution of muropeptide fragments. Thus, observing reproducible distributions of muropeptide fragments following double-digestion leads directly to the

identification of characteristic cleavage sites for the PG hydrolase of interest. While co-crystallization of proteins, with their cognate substrate is the most definitive method for determining protein substrate interactions, no structures of this class of amidase bound to substrate have been reported. Because co-crystallization has proven difficult, *in silico* docking methods have been utilized to propose potential protein/PG interactions (Chou *et al.* 2012). Thus, muropeptides have proven to be of limited use for binding assays (Mellroth *et al.* 2014).

Our long-term goal is to elucidate the molecular details of PG binding by PG amidases, and thereby contribute to the understanding of the antibiotic action of this class of enzymes. The current work was carried out on the toxic amidase effector 1 (Tae1) from *Pseudomonas aeruginosa*. While bacterial cells employ several "housekeeping" amidases that are responsible for remodeling the PG for bacterial cell growth, they are highly regulated (to prevent toxicity) and have very closed or occluded active sites (Figure 5) making structural imaging of these enzymes with PG substrates difficult (Chou *et al.* 2012).

Pseudomonas aeruginosa engages in interbacterial "chemical warfare" using a secretion system known as Type Six Secretion (T6S) to deliver toxic effectors to neighboring bacterial cells, thereby providing it a significant competitive advantage (Russell *et al.* 2011).

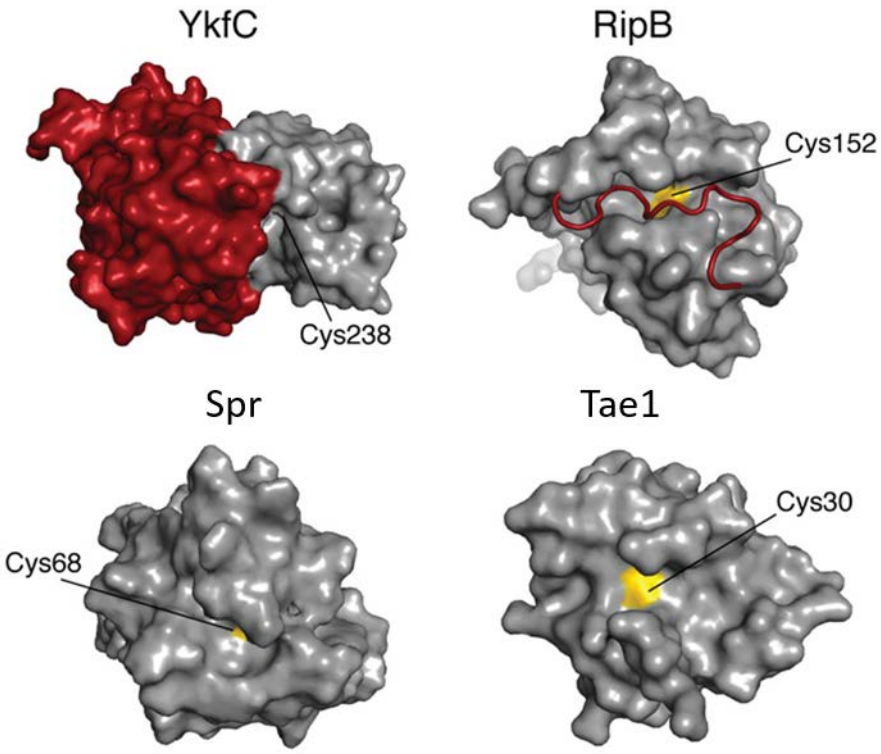

Figure 5: X-ray crystal structures of closest structural homologs "housekeeping" PG amidases and Tae1. Catalytic cysteines are highlighted in yellow, and regulatory regions are highlighted in red. PDB entries 3H41, 3PBI, 2K1H, and 4F4M respectively. Note the active-site-proximal regulatory region of the non-toxic amidase YkfC (red). Further, it can be seen that RipB contains an N-terminal extension (red) and Spr has catalytic-site adjacent residues that occlude their substrate binding sites relative to that of the toxin Tae1. See "Figure 2A" from Chou et al 2012, "Structure of a Peptidoglycan Amidase Effector Targeted to Gram-Negative Bacteria by the Type VI Secretion System", Cell Rep. *2012; 1(6):656-64.*

As shown in Figure 6, type six secretion (T6S) in *P*. *aeruginosa* cell requires the assembly of a long actin filament tubule akin to a bacterial sex pilus (Russell *et al.* 2011). Upon contact with a neighboring cell the tubule is rapidly shot out of the host cell piercing the neighboring cell like a hypodermic needle (Russell *et al.* 2011). A host of

toxic effectors are then injected through the T6S assembly (Russell *et al.* 2012). These toxic effectors are delivered via direct translocation through the phage-like apparatus (Russell *et al.* 2011).

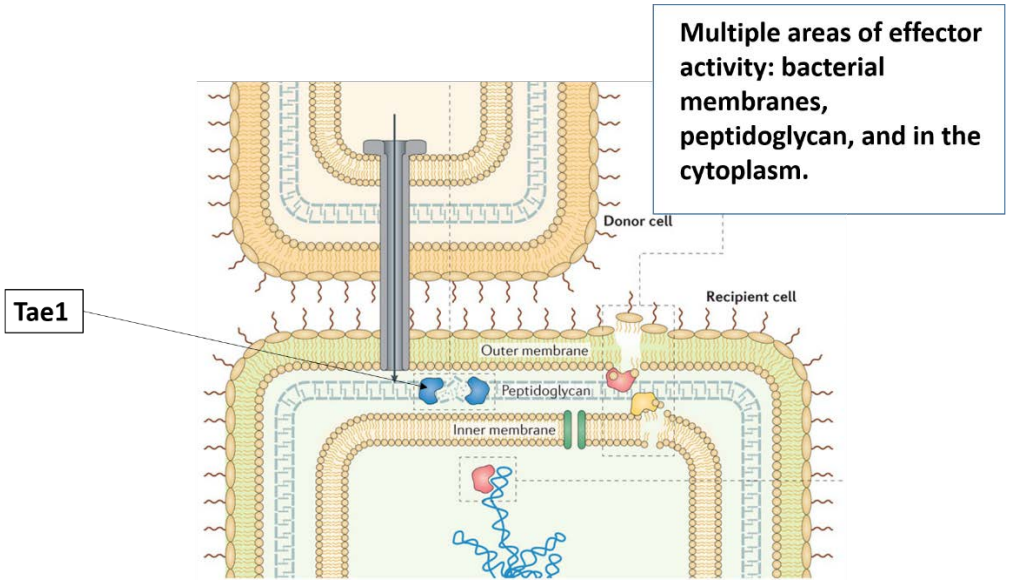

Figure 6: Cartoon representation of type six secretion with host cell piercing outer membrane of neighboring cell and injecting toxic effects. See "Figure 1" from Russell, et al (2014) "Type VI secretion effectors: poisons with a purpose" Nature Rev. Microbiol. 12: 137-148.

In addition to addressing questions of the mechanism of the effectors themselves, we hope to understand how the effectors are localized to the T6S and thereby secreted. Given the variety of proteins in the cytoplasm, how do secretion systems such as T6S discriminate between them and exclusively bind and secrete the appropriate effectors? Such substrate specificity might be mediated by several factors including signal sequences, chaperones, and receptors (Silverman *et al.* 2013).

Studies by the Mougous lab at UW Microbiology implicated the ring structured haemolysin coregulated protein 1 (Hcp1) in the localization and excretion of the type six secretion system effectors (Silverman *et al.* 2013). While initially thought of as a "static conduit" through which effectors of the T6S would pass, Hcp1 was shown to have a significant impact on both the cytoplasmic concentration of the toxic type six secretion effector 2 (Tse2) and its excretion (Silverman *et al.* 2013). To perform studies on the export of effector proteins the ΔretS mutation was incorporated which results in the excretion of effectors directly into the supernatant (Silverman *et al.* 2013). By doing this, effectors and cofactors necessary for excretion could be identified.

When Hcp1 is knocked out, the effectors Tae1, Tse2, and Tae3 are not found in the supernatant in measurable quantity (Silverman *et al.* 2013). Along with full gene knockout, structural mutations that effect the internal binding residues, such as the S115Q mutation, stop exportation of the toxic effectors (Silverman *et al.* 2013). Further investigation utilizing transmission electron microscopy (TEM) found that Tse2 was found localized and bound within the Hcp1 ring structure (Figure 7; Silverman *et al.* 2013). While it was not explicitly shown that Tae1 and Tae3 were bound within the Hcp1 ring, the secretion data cited above, and TEM findings of Tse2 bound to Hcp1 suggested that Tae1 binds with Hcp1 and is thereby exported through the T6S (Silverman *et al.* 2013). Thus, we performed NMR titration experiments with ^{15}N-labeled Tae1 and unlabeled Hcp1 in an attempt to identify the contacts between the two proteins.

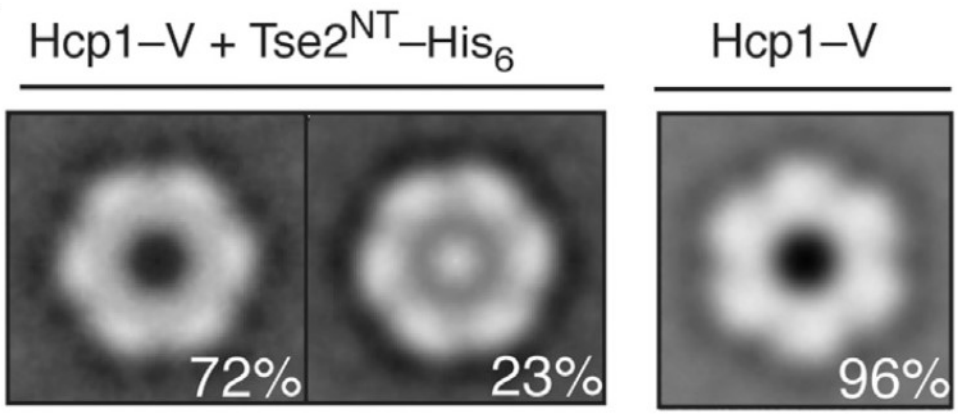

Figure 7: TEM images of Hcp1 showing the distribution of class averages in a sample of 3,000 randomly selected particles with 72% unfilled, 23% filled; additionally displayed is a control of Hcp1 not incubated with Type six secretion effector 2(Tse2), displaying that the filled particles are indeed bound with Tse2. See "Figure 3D" from Silverman et al 2013 "Haemolysin Coregulated Protein Is an Exported Receptor and Chaperone of Type VI Secretion Substrates," Annu. Rev. Microbiol. 2012; 66: 453-72.

Tae1 and Tae3 have been shown to be lytic enzymes with Tae1 breaking down the crosslinked peptide region of the peptidoglycan and Tae3 showing muramidase activity, cleaving between the glycans in the PG backbone (Chou *et al.* 2012). These peptidoglycan hydrolases were found through a heuristic investigation to be part of a superfamily of toxic effectors which cluster into conserved branches, each with a distinct PG cleavage specificity (Figures 8 and 9; Russell *et al.* 2012).

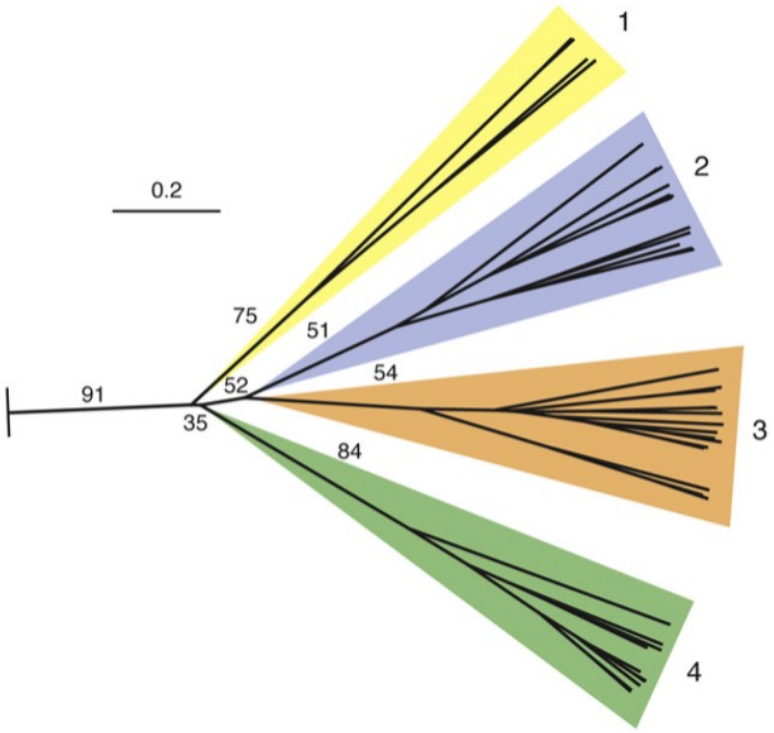

Figure 8: Type six secretion amidase effectors can be broken into 4 family groups distinguished by their peptidoglycan cleavage specificity. See "Figure 3C" from Russell et al 2012 "A Widespread Bacterial Type VI Secretion Effector Superfamily Identified Using a Heuristic Approach," Cell Host Microbe. 2012; 11(5): 538-49.

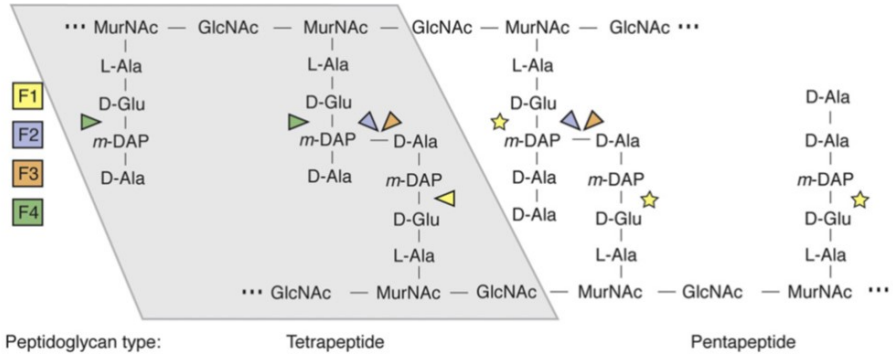

Figure 9: Sites of PG cleavage by the distinct amidase families. The color coding is the same as in Figure 8. Tips of color coded triangles point to scissile bond within the PG. See "Figure 4B" from Russell et al 2012 "A Widespread Bacterial Type VI secretion Effector Superfamily Identified Using a Heuristic Approach," Cell Host Microbe. 2012; 11(5): 538-49.

The observation of conserved cleavage specificities is intriguing given their roles as toxins. More promiscuous cleavage would, in principle, inflict greater damage to the cell wall target. The PG substrates needed to determine the observed cleavage specificities are obtained from bacterial saccule. First bacterial peptidoglycan sacculi are extracted from the rest of the bacterial cell by breaking apart the primary cell components with a bead beater, followed by sedimentation of the cell walls with high speed centrifugation, then enzymatic digestion of the remaining non-peptidoglycan elements with RNase, DNase, and Trypsin. Extracted sacculi are then treated with the given effector amidase followed by a glycan-degrading muramidase so that the remaining muropeptide fragments can be analyzed by HPLC-MS to determine where in the PG amidase directed hydrolysis occurs as seen in Figure 10 (Russell *et al.* 2012). Due to the difficulty of working with whole PG sacculi, digesting the PG macromolecule into muropeptides for further investigation is necessary for structural or binding studies (Kühner *et al.* 2014)

Tae1 was found to be specific for cleavage of the γ-D-glutamyl-L-*meso*-diaminopimelic acid (D-glu-*m*-*dap*) bond, indicated by the green arrowheads in Figure 10 (Chou *et al.* 2012). By the HPLC-MS experiments displayed in Figure 10 one can observe that PG fragment products obtained after double digestion of sacculi with Tae1 followed by muramidase define a high cleavage specificity of Tae1 for the D-glu-*m*Dap bond. Given this cleavage specificity, *B. subtilis* was used as the bacterium of choice for the isolation sacculi to be used as a test substrate for probing the details of Tae1 binding

to PG. *B*. *subtilis* is a well-studied gram positive bacterium, and its PG layer contains the necessary (D-glu-*m*-*dap*) bond.

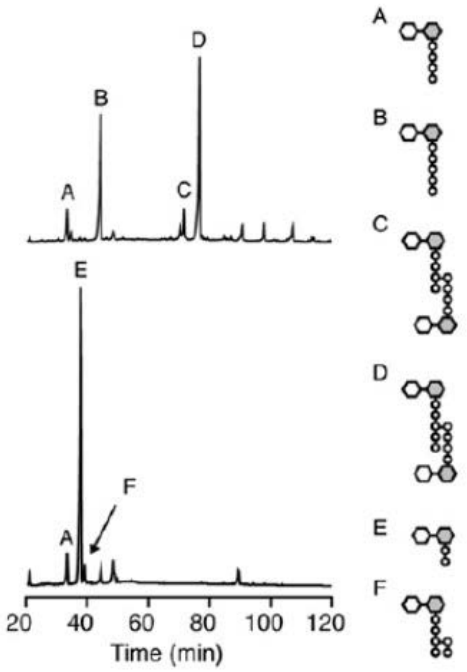

Figure 10: HPLC chromatograms of PG sacculus treated with the muramidase cellosyl (top) and PG sacculus treated with Tae1 followed by cellosyl (bottom). See "Figure 4A" from Chou et al 2012 "Structure of a Peptidoglycan Amidase Effector Targeted to Gram-Negative Bacteria by the Type VI Secretion System," Cell Rep. *2012; 1(6):656-64.*

The crystal structure of Tae1 has been solved to 2.6 Å resolution (Figure 11; Chou *et al.* 2012). As seen in Figure 11 the active site is very open, suggesting multiple orientations of PG are possible. Attempts to co-crystallize various PG substrates with Tae1 have not yet yielded crystals that diffract (Chou *et al.* 2012, Shang *et al.* 2012). Docking studies performed *in silico* using MacroModel 9.9 to scan the structural face of Tae1 with an L-Ala-D-Glu-mDAP PG fragment did not converge on a common bound conformation in the catalytic pocket of Tae1, but rather, returned 168 unique

conformations with 20 of them sharing the highest score from the Glide XP function (Chou *et al.* 2012). Thus, while the specific site of cleavage within the peptidoglycan and the structure of Tae1 are known explicitly, the interactions that determine the cleavage specificity of Tae1 remain unknown.

This prompted us to ask whether solution-state Nuclear Magnetic Resonance spectroscopy (NMR) might reveal the molecular features of Tae1 that lead to the observed cleavage specificity.

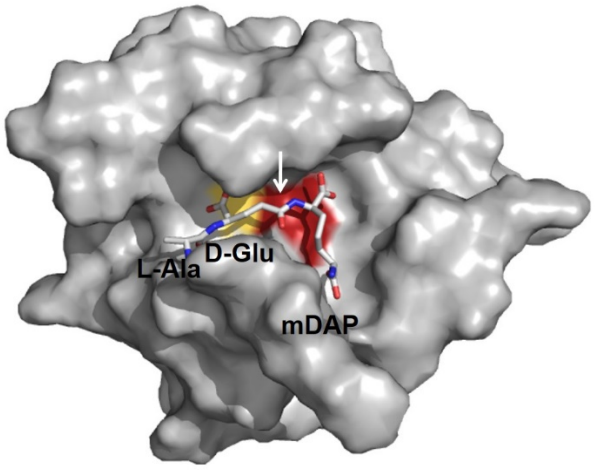

Figure 11: Tae1 crystal structure a fragment of PG modeled in the binding cleft in one possible conformation within the active site. Catalytic residues Cys30 and His91 labeled yellow and red respectively.

For proteins the relationship between structure and function is well-established thanks to the molecular-level insights provided by X-ray crystallography and NMR (Ziarek *et al.* 2011). X-ray crystallography is the gold standard for protein structure determination, however it has multiple limitations. Its greatest limitation is the necessity of crystallization of the protein and substrate (Williamson *et al.* 2013). To

analyze the structure of proteins in solution NMR is the superior technique. NMR is limited in its application by the size of the analyte. At ~ 17kDa, Tae1 at it is well within the range of molecular weights for which NMR is tractable (Cavanagh *et al.* 2010).

NMR relies on the nuclear spin of atoms with odd mass numbers in that such nuclei have magnetic moments. Within a strong external magnetic field (B_0) the nuclear magnetic moments will align with that of B_0. Nuclear magnetic moments exhibit Larmor precession around the axis of the external magnetic field as shown in Figure 12. The greater the strength of B_0 the higher the frequency of the precession.

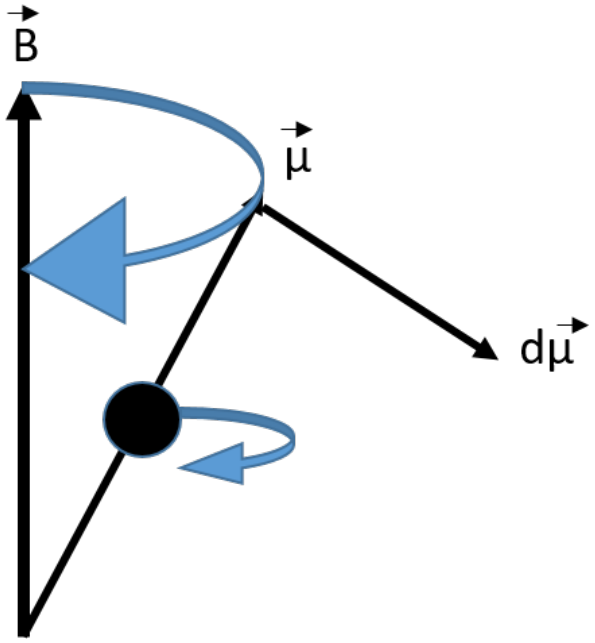

Figure 12: Larmor precession of nuclear spins in an external magnetic field.

The Larmor precession of the individual nuclear spins in the protein cannot be observed directly (Cavanagh *et al.* 2010). The individual precessing magnetic moments of the various nuclei sum together to form a single vector in the direction of B_0 (Cavanagh *et al.* 2010). To observe the nuclear magnetization we must force the

magnetization perpendicular to B_0. This is achieved by applying a radio pulse with the same frequency as the Larmor precession (Cavanagh *et al.* 2010). After the pulse, the nuclear magnetization vector will then be perpendicular to the external magnetic field and the angular rate of rotation will induce an electric current which can be measured in a receiver coil surrounding the sample (Hore *et al.* 2000). Over time the perpendicular magnetization will decrease as the magnetization relaxes to align with B_0 (Cavanagh *et al.* 2010). Thus, the amplitude at the receiver coil will decrease over time and provide a measurement known as the free induction decay, or FID (Figure 13; Hore *et al.* 2000).

By applying a Fourier transform (FT) to the FID one is able to deconvolute the FID into a dataset that resolves the resonance frequencies for individual nuclei (Cavanagh *et al.* 2010). The NMR active nuclei of the molecule exist in different chemical environments and thus can be distinguished from one another by their characteristic chemical shifts (Cavanagh *et al.* 2010). In the work described herein, we are exploiting the fact that changes in the local chemical environment, such as protein-substrate binding, are associated with changes in the local magnetic environment of a given nucleus. This is manifested as a change in the chemical shift for that nucleus, and is the key piece of information needed to map which atoms in the protein are likely involved in substrate binding.

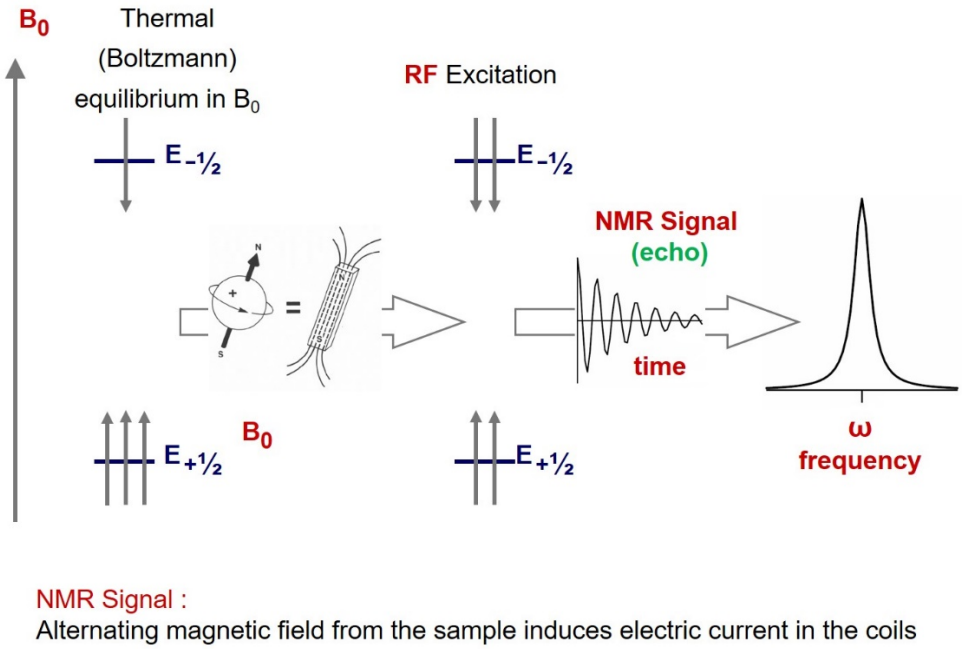

Figure 13: NMR data workflow. Image generated by Dr. Serge Smirnov at Western Washington University, Department of Biochemistry.

Figure 14 shows a one-dimensional (1D) spectrum of ^{1}H resonances for the 76-residue peptide ubiquitin. As is evident from Figure 14, there is substantial overlap in the resonances of the 629 ^{1}H nuclei in ubiquitin in a 1D NMR spectrum, making the resolution of individual resonances impossible. To achieve resolution of these signals so-called multi-dimensional experiments are necessary.

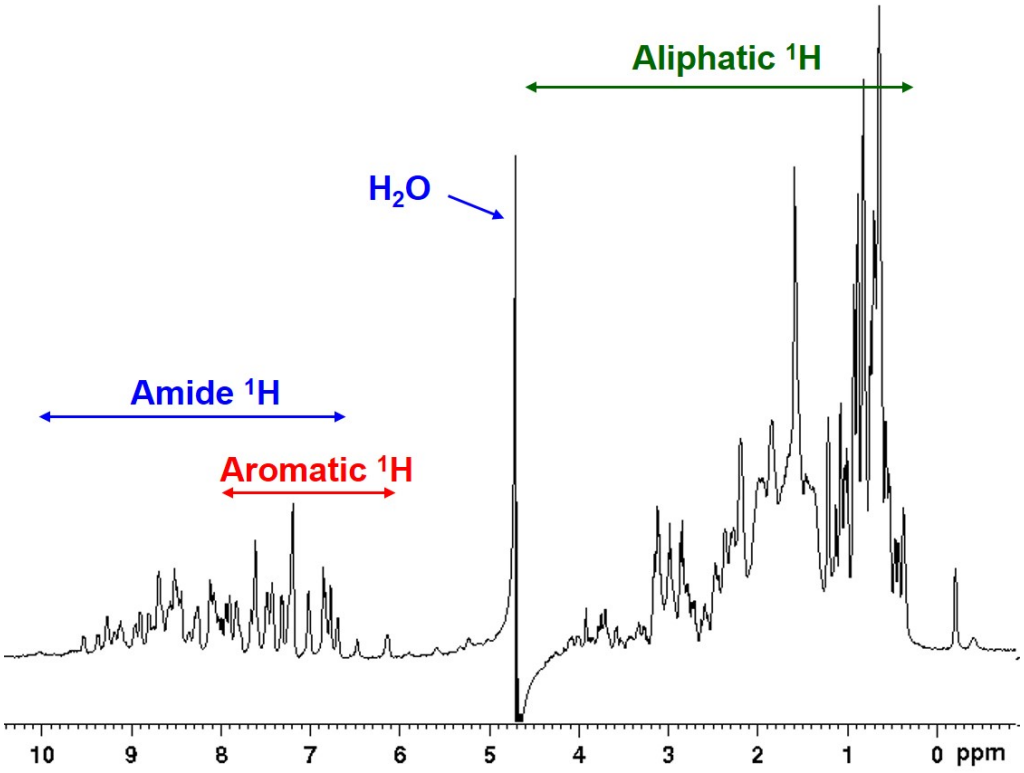

Figure 14: 1D 1H-NMR spectrum of the small protein ubiquitin. The spectrum was acquired on a 500 MHz instrument. The ranges of chemical shifts for aliphatic, aromatic, and amide protons are indicated. Mathews et al. "Biochemistry 4th edition", pg 225.

To perform a multi-dimensional experiment it is necessary to enrich the protein in the NMR-active nuclei ^{15}N and/or ^{13}C, both of which are present in low natural abundance. Figure 15 shows the amide ^{1}H resonances for ubiquitin resolved in a two dimensional NMR experiment (^{15}N-HSQC) that records individual ^{1}H spectra as a function of ^{15}N chemical shift. The individual backbone amide ^{1}H resonances can be completely resolved using this approach. For larger proteins there may be overlap of resonances in the ^{15}N HSQC. Individual resonances can then be resolved by collecting a 3D dataset which includes a series of ^{15}N HSQC spectra recorded as a function of ^{13}C

chemical shift. Such 3D datasets are also need to assign the individual resonances in the HSQC spectrum to particular amino acids in the protein sequence.

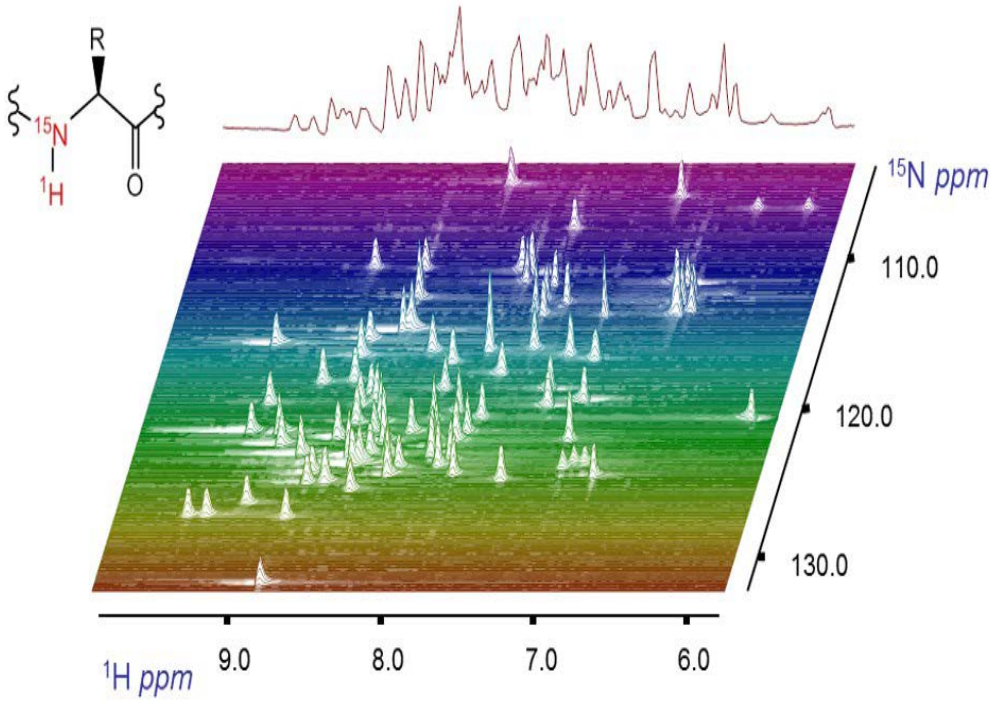

Figure 15: Display of 2D Protein NMR experiment. Due to the complexity of proteins it is necessary to utilize multi-dimensional experiments. A proton spectrum is collected at each nitrogen shift. If compiled together into a single proton spectrum the amount of data is overly convoluted. By working with the data in two dimensions it is possible to resolve the peaks and gain valuable information for each residue. Most commonly this is imaged from the top down as a topographic map as shown in Figure 16. Mathews et al. "Biochemistry 4th edition", pg 226 (Figure generated by S. Smirnov).

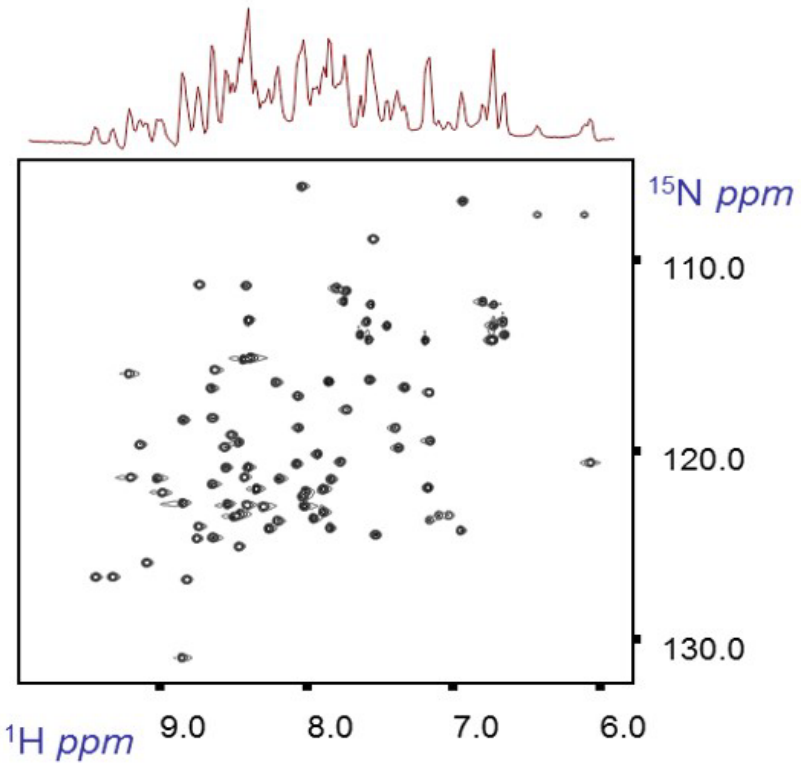

Figure 16: 2D NMR top down "topographical" map view of a standard NHSQC where each spot is a peak from the two dimensional spectrum. Mathews et al. "Biochemistry 4th edition", pg 226 (Figure generated by S. Smirnov).

The changes in the chemical environment of the protein upon binding of a specific substrate lead to changes in the positions and intensities of peaks in the HSQC spectrum (Cavanagh *et al.* 2010). Depending on the relative rates of ligand binding and NMR data acquisition, the changes to the peaks in the HSQC spectrum will be observed in different ways. If the association of the protein and its ligand occurs faster than the NMR acquisition time, a shift in the peak is observed (Hole *et al.* 2000). If instead the rates of ligand binding and release occur on the same timescale as the NMR acquisition time, peak broadening will be observed (Hole *et al.* 2000). Finally, if the ligand binding/release is slower than the NMR acquisition time, a peak doubling will occur

(Hole *et al.* 2000). The changes in peak position and/or intensity can be used to map the sites on the protein that are most affected by ligand binding.

For an NMR investigation of the interaction between an enzyme which cleaves its substrate, such as Tae1 and peptidoglycan, it is necessary to inhibit the activity of the enzyme to allow for NMR data collection on a homogenous sample. (Cavanagh *et al.* 2010). If Tae1 maintains its amidase activity then the interaction between Tae1 and PG will be over too quickly for observation by NMR. To get around this problem a point mutation was made which inactivates the enzyme by replacing the essential cysteine nucleophile with alanine. This mutation does not otherwise effect the structure of the protein (Vivian *et al.* 2003). Unfortunately, this mutation did not facilitate the co-crystallization of Tae1 with PG fragments. Nevertheless, we hope to use NMR to determine which residues in Tae1 are responsible for PG binding.

Methods

Tae1 containing a C-terminal hexahistidine tag was expressed and purified as described (Chou *et al.* 2012). Briefly, soluble protein was isolated from clarified lysate by metal affinity chromatography followed by size-exclusion chromatography

PG fragments were isolated from *B*. *subtilis*. Both liquid media and plate growth were attempted to determine best method for bacterial production. For plate growth *B*. *subtilis* seed stock was inoculated on rich plate media and held in a constant temperature incubator overnight. Subsequently the bacterial colonies were scraped off of the plates with a glass stir rod and ice cold saline and collected in a flask. Liquid media growth was performed in LB medium inoculated with *B*. *subtilis* seed stock and held overnight in a constant temperature shaker.

In both cases once the growth was complete bacterial cells were harvested by high speed centrifugation with two washes of cold sodium chloride solution, one of water, and three final washes with acetone. Subsequently the washed cell pellet is dried at 37^{o}C. The dried bacterial cells are then suspended in ice-cold water and transferred to 2mL "bead beater" tubes containing roughly five 0.10-0.15mm glass beads. These samples are then treated in a bead beater for four two-minute intervals for a total of 8 minutes with cooling on ice for 6 minutes in between rounds. The mixture of broken cells and glass beads is filtered. The cell walls are then separated from the supernatant by ten minutes of centrifugation at 1500 x g and 4 ^{o}C. The pelleted cell walls were washed three times with water, and then resuspended in 200 mL of pH 7.6 phosphate buffer. To this suspension RNase A was added to a final concentration of 100

μg/ml, DNase to a final concentration of 50 μg/mL, along with 0.5mL toluene. This mixture was then incubated at 37 ^{o}C for 18hr at which point sterile trypsin was added to a final concentration of 200 μg/ml and incubated for a further 18 hours at 37^{o}C. After the final incubation period the cell walls were pelleted by high speed centrifugation as described above, washed three times with water, and finally lyophilized.

NMR data was collected on a 500 Mhz Bruker instrument in the lab of Rachel Klevit. Data was processed with NMRpipe using scripts provided by Dr. Peter Brzovic.

NMR assignment was performed utilizing the "NMRviewJ" software suite from One Moon Scientific. Assignments of backbone amides in the NHSQC spectrum, were carried out by analysis of data from HCONH, HNCACB, HNCB, and HCCONH experiments. For the side chain assignments, HCCH COSY and HCCH TOCSY peaks were individually peak-picked and assigned by hand. Multiple attempts were made to achieve the best assignment possible for the CHSQC using combinations of the ppm assignments from the previously assigned side chain experiments. Side chain assignments were checked against average values from the Biological Magnetic Resonance Bank (BMRB; http://www.bmrb.wisc.edu/). This initial assignment was checked further utilizing the NMRviewJ "atom assign" tool. Each assignment was also checked against the X-ray crystal structure to make sure that the proposed assignments fell within established ranges for a given residue in the context of the predicted secondary structure.

A typical assignment workflow requires working through a single sidechain at a time, cross-referencing the paired experiments (i.e., HCCH TOCSY and HCCH COSY) to make sure that the assignments match. Due to the high number of shared resonances

between similar amino acid side chains it was helpful to resolve these shared resonances by comparing residue assignments with the location found in the X-ray crystal structure and against BMRB standards. A typical assignment for a single side chain can take several hours to complete. For the NMR titration analysis, the changes in peak intensity for each resonance are graphically compared, normally after their overall change has been normalized to one, as observed in Appendices 4 and 5.

Results

The initial characterization of Tae1 assigned 89.2% of the backbone amides and 87.4% of side chains, Figures 17-20. Factors that limit the completion of assignments include the absence of peaks for prolines, and the inability to differentiate between reciprocal/mirror-imaged systems (such as the two delta carbons and 6 delta hydrogens found in Leucine). In these cases, the peak in the spectrum was labeled with a shared assignment. Of the non-assigned residues displayed in grey in figures 17 and 18, there are six proline residues, furthermore the unassigned active site proximal extension is composed of Thr88 and Tyr89, and the unassigned residue to the far right of the catalytic His91is Arg132. As the backbone assignments are necessary for sidechain assignment, the percentage of residues with backbone assignments represents the upper limit of what can be achieved for sidechain assignments. Therefore, 87.4% side chain assignments represents a nearly full coverage of all assignable sidechain residues in NMR experiments. These assignments set the stage for investigating the binding of Tae1 with Hcp1 and peptidoglycan.

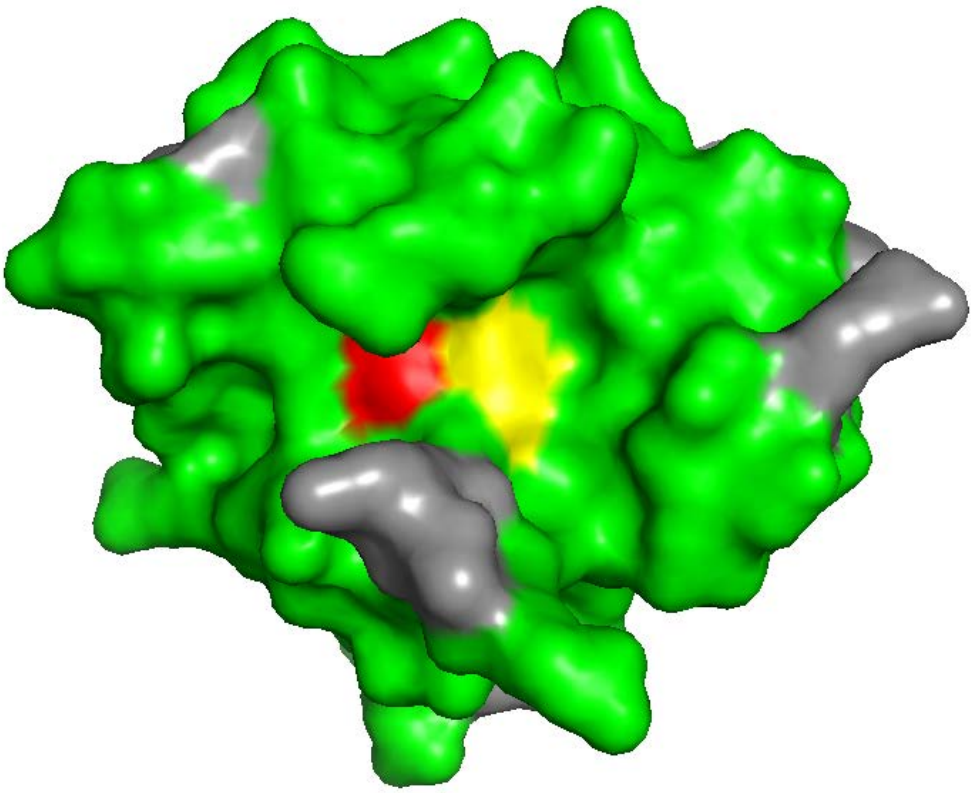

Figure 17: Pymol image of Tae1 with assigned backbone residues colored in green, and unassigned residues colored in grey. Catalytic residues Cys 30 and His 91 colored red and yellow respectively

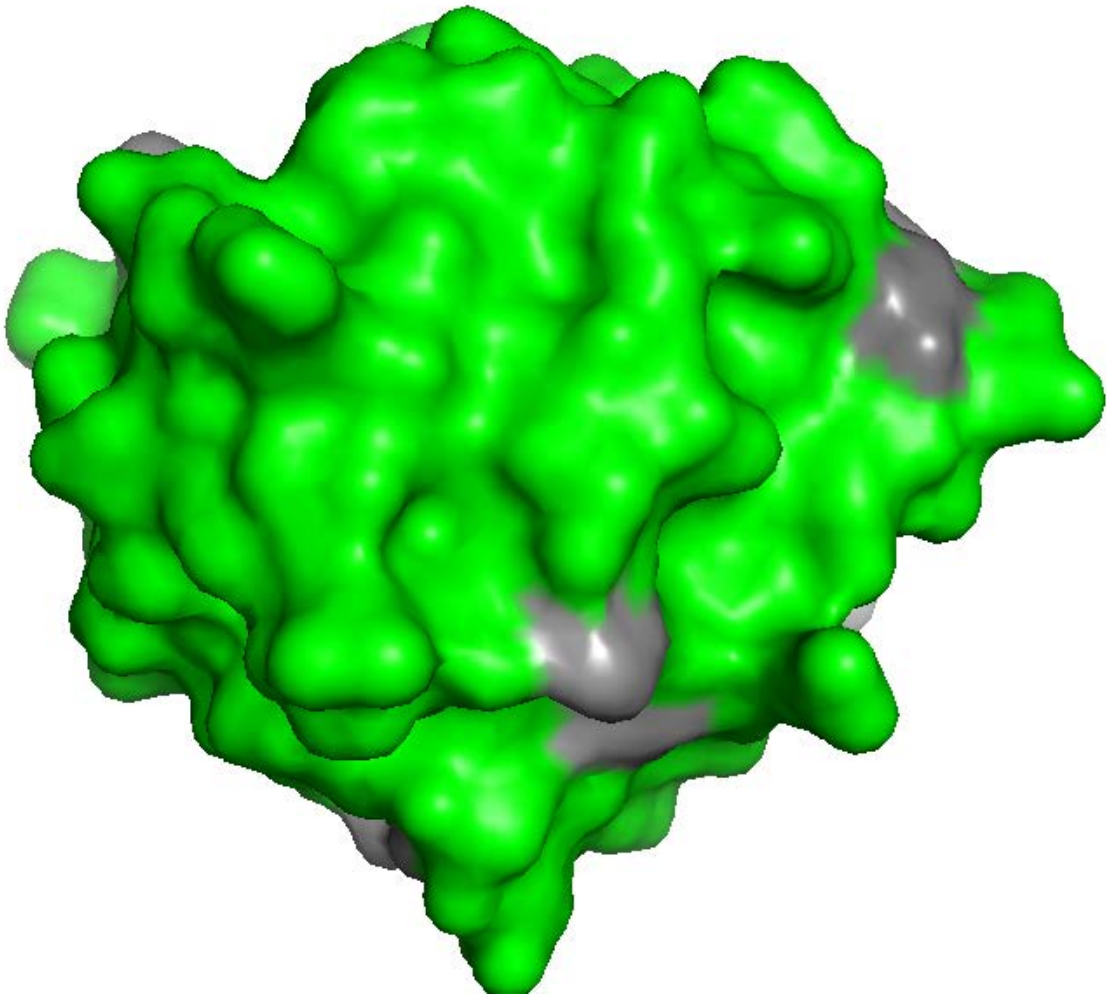

Figure 18: Pymol image of the backside of Tae1 with assigned backbone residues colored in green, and unassigned residues colored in grey.

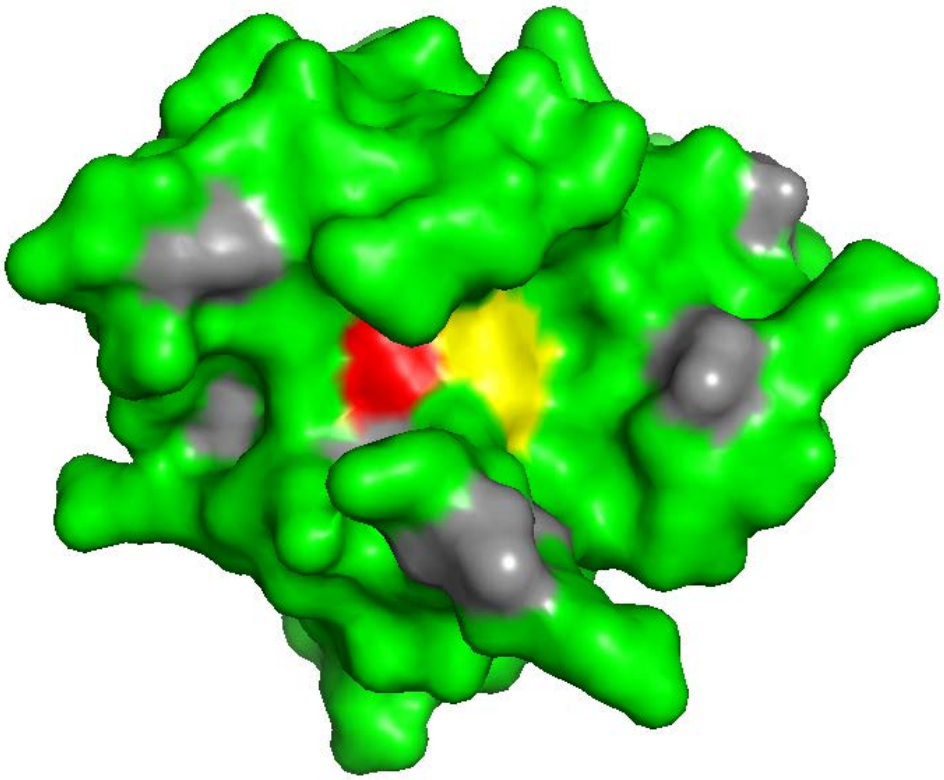

Figure 19: Pymol image of Tae1 with assigned side chain residues colored in green, and unassigned residues colored in grey. Catalytic residues Cys 30 and His 91 colored red and yellow respectively

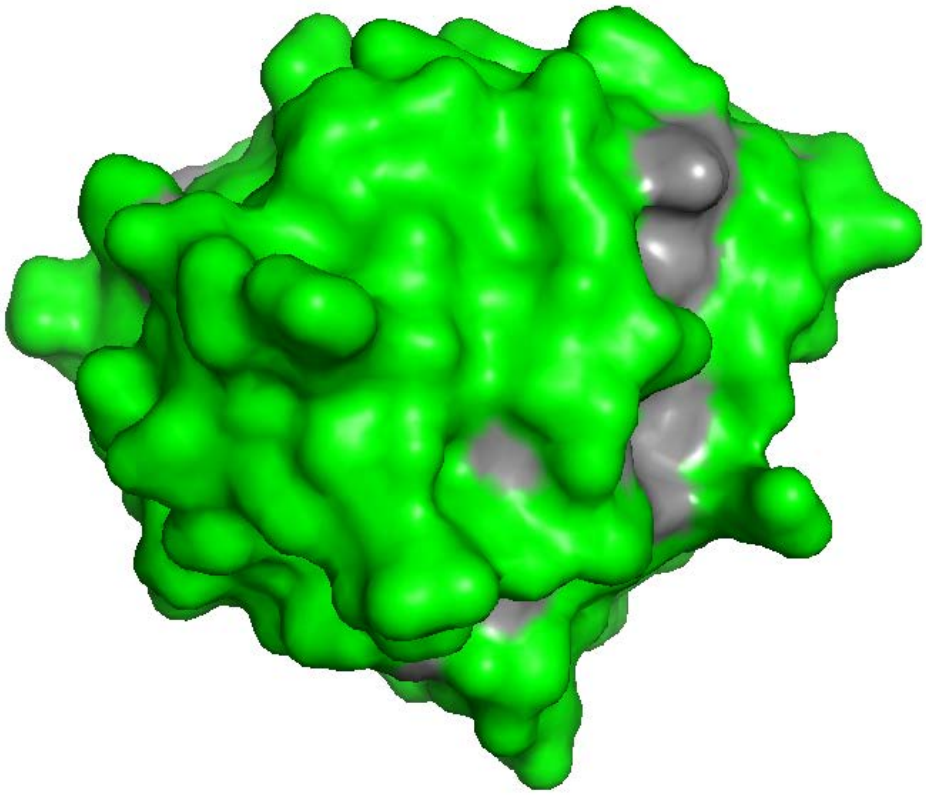

Figure 20: Pymol image of the backside of Tae1 with assigned side chain residues colored in green, and unassigned residues colored in grey

After the assignment of the backbone amides for Tae1 an NMR titration was performed by incubating ^{15}N-labeled Tae1 with increasing concentrations of Hcp1 (Figure 21) and the non-binding Hcp1 mutant S115Q, with the expectation that the addition of increasing wild type Hcp1 would affect certain Tae1 resonances, whereas the S115Q mutant would not show any effect (Silverman *et al.* 2013). As can be observed in figure 22 and 23 there were little to no observable changes in the spectra through the series of the titrations. Shown in Appendix 4 and 5 are the graphical analyses of the titrations which show that the only quantitative change is a decrease in overall spectral intensity as a function of increasing concentrations of Hcp1.

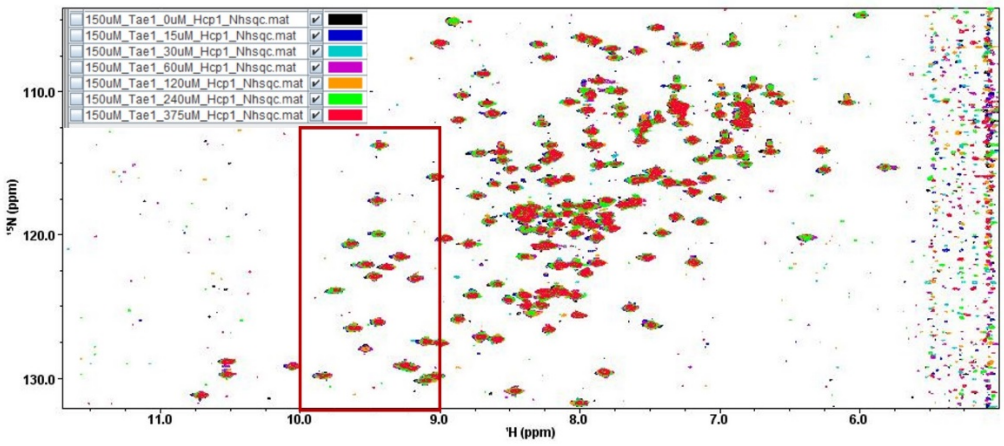

Figure 21: NHSQC overlay of Tae1 titration with Hcp1. The red box displays the region of the spectrum utilized in Figures 22 and 23

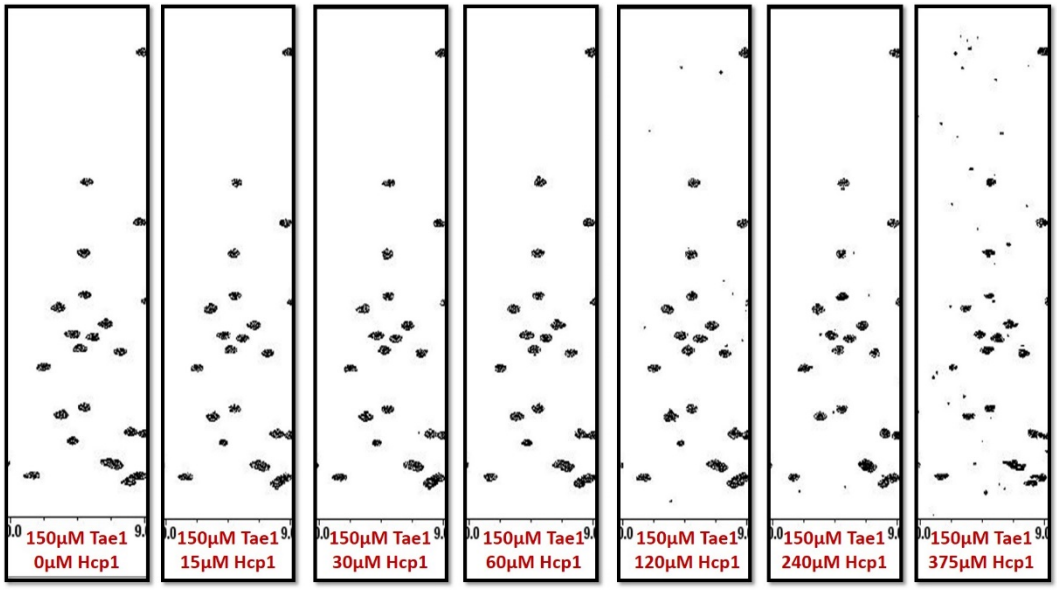

Figure 22: Representative panels from NHSQC titration of Tae1 with increasing concentrations of Hcp1

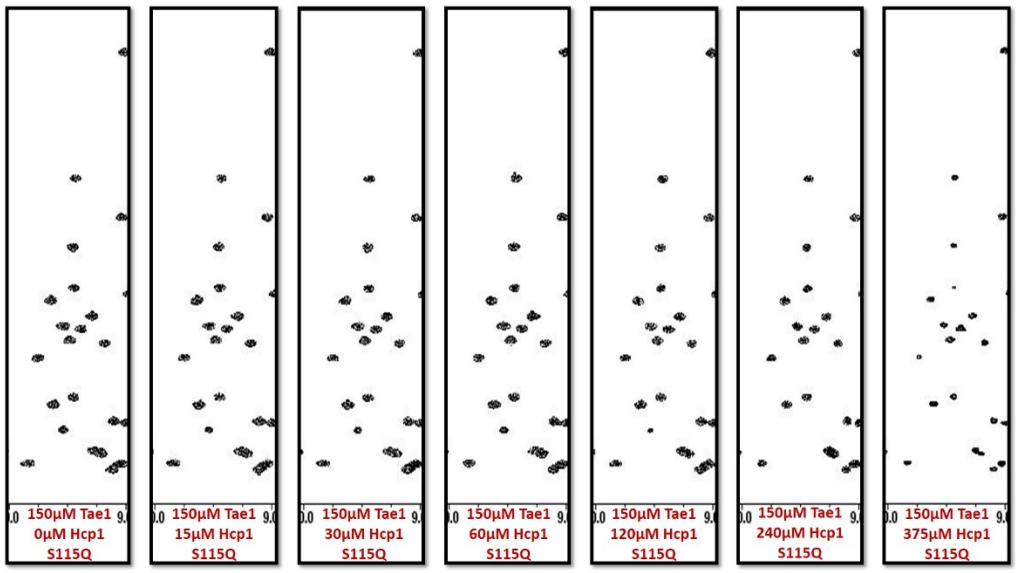

Figure 23: Representative panels from NHSQC titration of Tae1 with increasing concentration of Hcp1 mutant S115Q.

To explore binding of Tae1 with it's putative substrate Tae1 titrations with a muropeptide containing the L-Ala-D-Glu-mDAP crosslink within a series of 9 residues with a single GlcNac moiety bound to the muropeptide known as the "tetra-tetra" fragment of PG (see figure 24) were also performed, but yielded no evidence for specific binding.

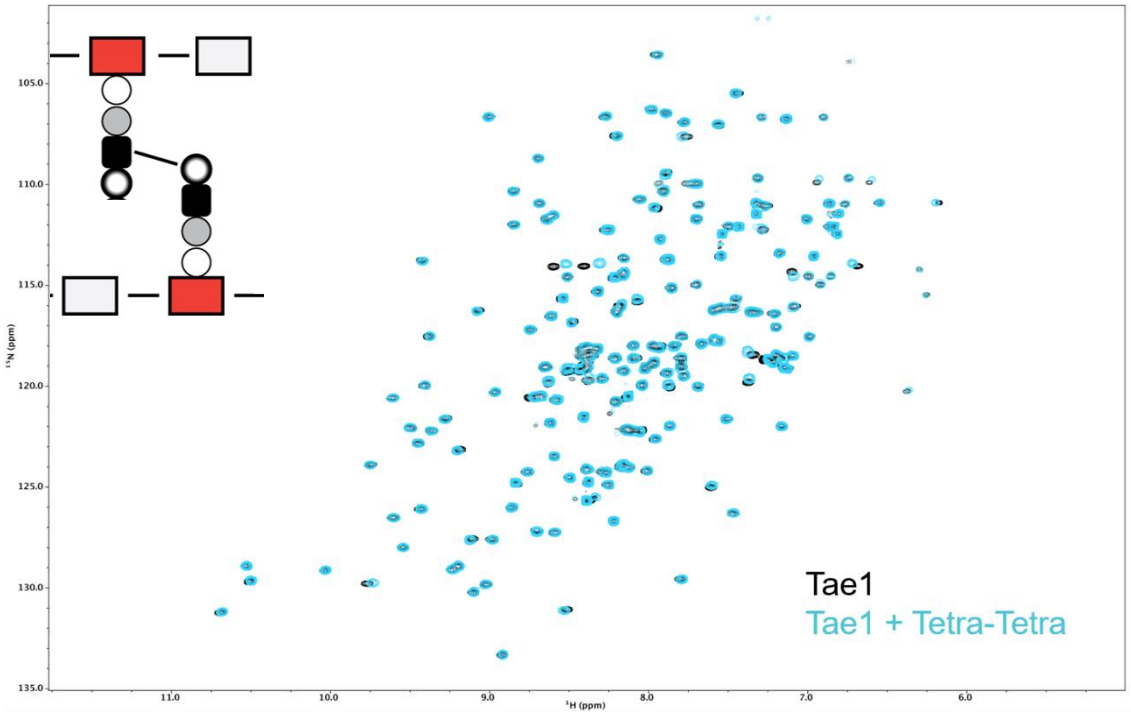

Figure 24: NHSQC overlay of Tae1 (black) and Tae1 incubated with tetra-tetra fragment (displayed in upper left corner of the spectrum) of PG (teal). Spectra collected by Drs Seemay Chou and Jonathan Pruneda at University of Washington.

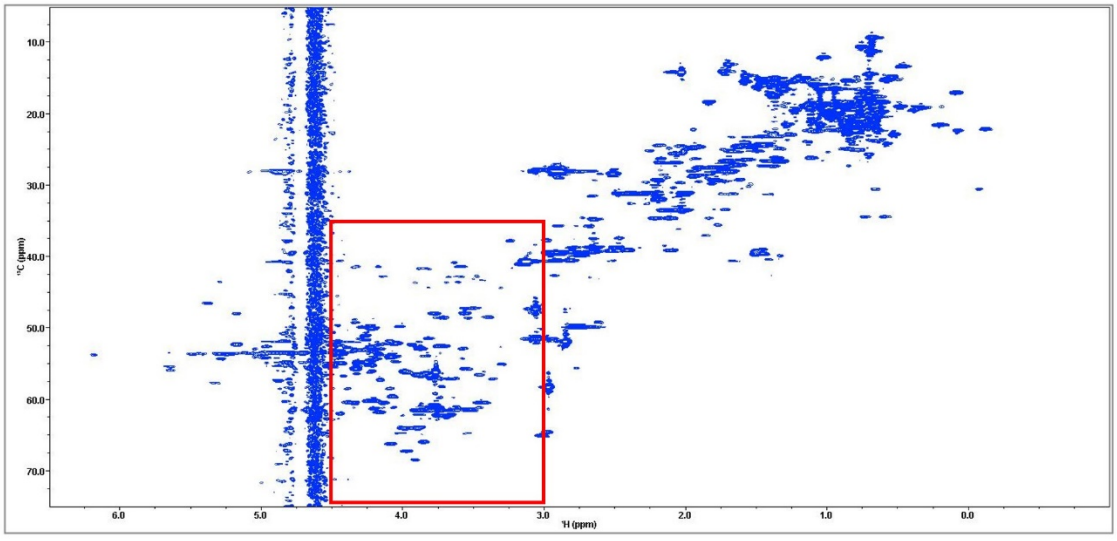

Figure 25: CHSQC of Tae1 with the spectral region displayed in figure 26 highlighted in red.

To generate side chain assignments, the CHSQC spectrum of Tae1 was assigned using the NHSQC assignments as well as C atom resonances observed in the following experiments: CCONH TOCSY, HCCONH TOCSY, HCCH COSY, and HCCH TOCSY. Owing to the vast amount of information on the CHSQC spectrum it was extremely difficult to resolve assignments for individual residues, however 70% of the peaks could be assigned, as shown in Appendix 2. This provided coverage of at least a portion of the protons for every single side chain residue that could be assigned (e.g., Pro residues are not assignable). While not every proton for each side-chain could be assigned, the spectral coverage of Tae1 in side chain displaying experiments is very robust.

Upon incubation of triple-labeled Tae1 with intact sacculi we observed several peaks disappearing from the spectrum. To investigate the role of the glycan strand in the binding, Dr. Chou subsequently incubated this sample with lysozyme. Interestingly when a CHSQC spectrum was collected, all of the peaks that disappeared returned following the lysozyme treatment (Figure 26).

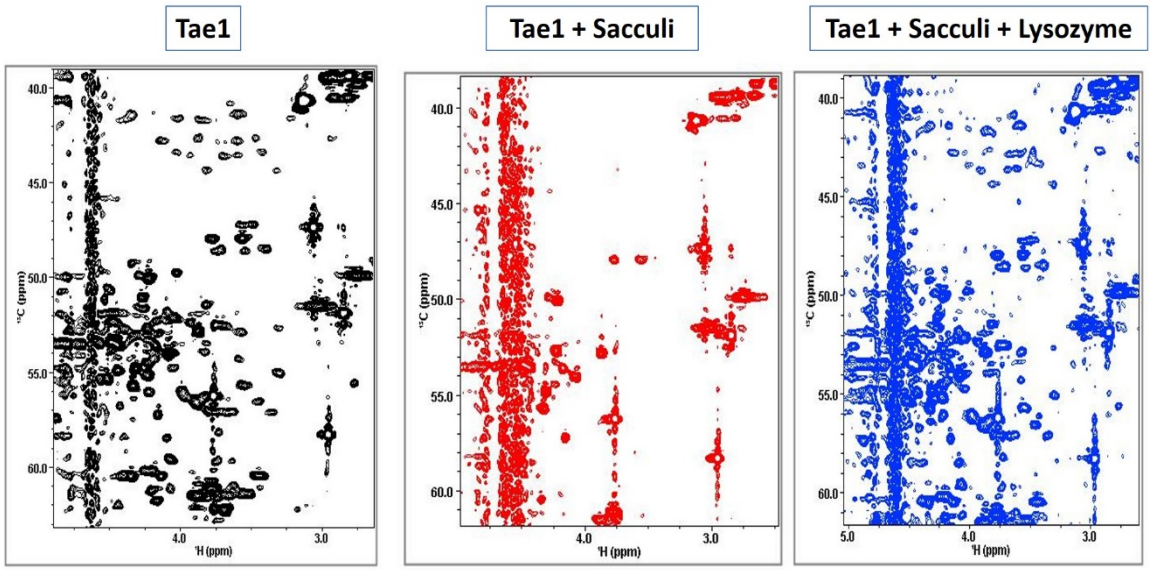

Figure 26: CHSQC spectra of Tae1 (black), Tae1 incubated with whole sacculi (red), and Tae1 incubated with whole sacculi then with lysozyme (blue)

Discussion

The experimental approach that we took for this project was the application of NMR to investigate the binding of the toxic amidase effector Tae1 with potential regulatory factor Hcp1 and Tae1's PG substrate. Our objective was to identify the residues of Tae1 which are responsible for determining the apparent specificity of PG cleavage by Tae1.

Standard NHSQC-based NMR titration experiments of PG fragments with Tae1 have not yet yielded any evidence that explains the apparent cleavage specificity of the amidase. Nor does Tae1 appear to bind Hcp1 with any specificity. Hcp1 had been shown to bind a different effector based on EM analysis, and given the role of Hcp1 in the

assembly of the secretion apparatus, we hypothesized that Tae1 would also associate with Hcp1 (Silverman *et al.* 2013).

The only evidence for binding in NHSQC-based experiments was observed at low pH (pH 5.0) for a side chain amide (Figure 24). We therefore turned to CHSQC experiments to probe the details of Tae1 side chain interactions with putative substrates.

CHSQC titrations show that the addition of intact sacculi results in the disappearance of several peaks; however, these peaks also showed a small signal to noise ratio prior to addition of the sacculi. Thus, differential effects on peak intensity of chemical shift were impossible to discern in this experiment. Interestingly, these peaks returned upon addition of lysozyme to this sample.

This result suggests that the glycan strand must be intact for Tae1 to bind. If this is true, it would explain the lack of specific interactions in the NHSQC titration experiments using PG fragments (in which the glycan portion was absent). Lysozyme cleaves PG between the GlcNac (NAG) and MurNac (NAM), but leaves the peptide region intact. We theorize that the binding affinity of Tae1 for PG is greater when the glycan strand is intact; however, it is unclear how (if at all) the glycan affects Tae1 cleavage specificity for the peptide portion of PG.

Intact sacculi are too large to allow us to probe specific interactions with Tae1 via NMR. PG fragments of defined size that include intact NAG-NAM bonds would be more amenable to NMR analysis; however, such fragments are not produced by the methods commonly used to generate PG fragments from sacculi.

Chemical synthesis has been used to generate defined PG fragments with intact glycan bonds. This method was utilized by Mellroth *et al.* however, this necessitated a thirty step synthesis which would be cost prohibitive for NMR-based investigations (Mellroth *et al.* 2014).

To generate appropriately sized PG fragments we have attempted fragmentation of purified PG sacculi through a combination of sonication and limited digestion with lysozyme. While this has not yet yielded the desired fragments, a future goal is to optimize this process to generate fragments of appropriate size and composition for NMR experiments.

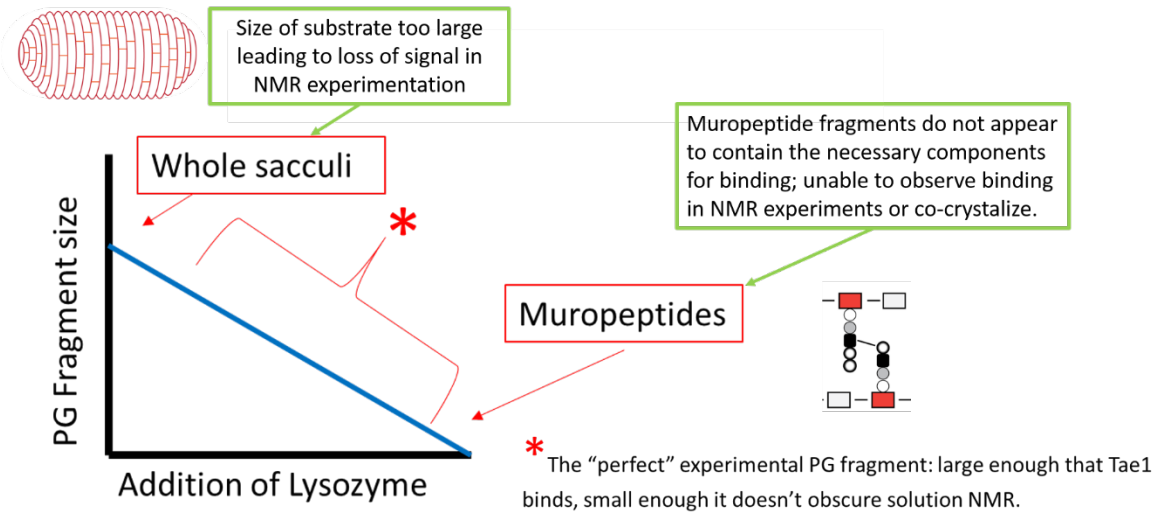

Figure 27: Cartoon representation of minimal binding fragment generation/isolation experiment theory. By utilization of stepwise addition of Lysozyme or sonication the goal will be to isolate fragments of a size small enough that they don't completely obscure the signal in NMR experiments as seen with intact sacculi, but with the necessary size and complexity that binding can occur and be observed.

In collaboration with the Vollmer lab, sacculi which have been treated with a muramidase (e.g., lysozyme) will be subsequently treated with catalytically active, wild-type, Tae1. As displayed in appendix 6, based on the results shown in Figure 10, we expect that this order of addition, muramidase then Tae1, will lead to reduced cleavage of the peptide portion of the PG. If significant cleavage of the PG peptides is observed in this experiment we would then need to examine whether the active site Cys to Ala mutation has impaired Tae1 binding to PG fragments compared to wild-type Tae1. The data in Figure 26 suggest that the presence of glycan strands in the PG fragments is required for Tae1 binding. A similar observation was reported by Mellroth *et al.* for the pneumococcal autolysin LytA (Mellroth *et al.* 2014). They found that having a GlycNac on both sides of the muropeptide was necessary for cleavage of PG by LytA. Furthermore, the cleavage of this PG fragment was reduced compared to cleavage of PG fragments with longer glycan strands. Upon further study, as reported in a recently released paper *in press*, Mellroth *et al.* successfully co-crystalized LytA with a large PG fragment (diGM5P) spanning four GlcNac/MurNac alternating residues linked to an L-Ala-D-Glu-L-Lys-D-Ala-D-Ala pentapeptide (Sandalova *et al.* 2016). This result supports our hypothesis of the necessity of a larger PG fragment for experimentally observable binding.

Solid state NMR (ssNMR) is a powerful technique which has been utilized in the study of PG and provided the first atomic model of an enzyme in complex with an intact bacterial PG sacculus (Schanda *et al.* 2015). Because of the size and dynamic nature of PG it is challenging to analyze large PG fragments via solution state NMR or X-ray

crystallography. Solid state NMR may be a useful method for future investigations of Tae1 interactions with larger PG fragments, however, the low sensitivity of ssNMR is of concern; while experiments showed effects within the PG from the binding of an L-D-transpeptidase from *B. subtilis* bound to its PG substrate the technique lacked the sensitivity required to determine atomic detail of the interaction of the protein itself (Schanda *et al.* 2015).

The challenges associated with the production/isolation of a suitable PG substrate of Tae1 have limited our ability to determine the atomic-level details of Tae1 binding to PG. However, our assignments of both the backbone and sidechain residues in Tae1 will allow for such determination as soon as a minimal binding fragment of PG can be isolated and characterized. Future work will be necessarily focused on development of such a minimal binding PG fragment.

Works Cited

1. Brown S., Santamaria J.P., Walker S. Wall teichoic acids of gram-positive bacteria. *Annu Rev Microbiol*. 2013; 67:313-36.

2. Cavanagh J., Fairbrother W.J., Palmer A.G., Skelton N.J., Rance M. Protein NMR Spectroscopy, Principles and Practice. Academic Press; 2010.

3. Chou S., Bui N.K., Russell A.B., Lexa K.W., Gardiner T.E., LeRoux M., Vollmer W., Mougous J.D. Structure of a peptidoglycan amidase effector targeted to Gram-negative bacteria by the type VI secretion system. *Cell Rep.* 2012; 1(6):656-64.

4. Desmarais, S.M., Cava, F., de Pedro, M.A., Huang, K.C. Isolation and Preparation of Bacterial Cell Walls for Compositional Analysis by Ultra Performance Liquid Chromatography. *J. Vis. Exp.* 2014; 83: e51183.

5. Gan L., Chen S., Jensen G.J. Molecular organization of Gram-negative peptidoglycan. *Proc Natl Acad Sci USA*. 2008; 105(48):18953-7.

6. Hore P.J., Jones J.J., Wimperis S. NMR, The Toolkit. Oxford University Press; 2000.

7. Kern T., Giffard M., Hediger S., Amoroso A., Guistini C., Khai Bui N., Joris B., Bougault C., Vollmer W., Simorre J.P. Dynamics characterization of fully hydrated bacterial cell walls by solid-state NMR: evidence for cooperative binding of metal ions. *J. Am. Chem. Soc.* 2010; 132(31):10911-9.

8. Kleckner I.R., Foster M.P. An introduction to NMR-based approaches for measuring protein dynamics. *Biochim Biophys Acta*. 2011; 1814(8):942-68.

9. Kühner D., Stahl M., Demircioglu D.D., Bertsche U. From cells to muropeptide structures in 24 h: peptidoglycan mapping by UPLC-MS. *Sci Rep*. 2014; 4:7494.

10. Lehotzky R.E., Partch C.L., Mukherjee S.,Cash H.L., Goldman W.E., Gardner K.H., Hooper L.V. Molecular basis for peptidoglycan recognition by a bactericidal lectin. *Proc. Natl. Acad. Sci. USA*. 2010; 107(17):7722-7.

11. Leroux M., De leon J.A., Kuwada N.J.,Russel A.B., Pinto-Santini D., Hood R.D., Agnello D.M., Robertson S.M., Wiggins P.A., Mougous J.D. Quantitative single-cell characterization of bacterial interactions reveals type VI secretion is a double-edged sword. *Proc. Natl. Acad. Sci. USA*. 2012; 109(48):19804-9.

12. Mellroth P., Sandalova T., Kikhney A., Vilaplana F., Hesek D., Lee M., Mobashery S., Normark S., Svergun D., Henriques-Normark B., Achour A. Structural and functional insights into peptidoglycan access for the lytic amidase LytA of Streptococcus pneumoniae. mBio. 2014; 5(1):1120-13.

13. Mathews C.K., Van Holde K.E., Appling D.R., Anthony-Cahill S.J. *Biochemistry*. Toronto: Pearson, 2013. Print.

14. Otero L.H., Rojas-Altuve A., Llarrull L.I., Carrasco-López C., Kumarasiri M., Lastochkin E., Fishovitz J., Dawley M., Hesek D., Lee M., Johnson J.W., Fisher J.F., Chang M., Mobashery S., Hermoso J.A. How allosteric control of Staphylococcus

aureus penicillin binding protein 2a enables methicillin resistance and physiological function. *Proc. Natl. Acad. Sci. USA*. 2013; 110(42):16808-13.

15. Romaniuk J.A., Cegelski L. Bacterial cell wall composition and the influence of antibiotics by cell-wall and whole-cell NMR. *Phil. Trans. R. Soc. B* 2015; 370(1679). http://dx.doi.org/10.1098/rstb.2015.0024

16. Russell A.B., Hood R.D., Bui N.K., Leroux M., Vollmer W., Mougous J.D. Type VI secretion delivers bacteriolytic effectors to target cells. *Nature*. 2011; 475(7356):343-7.

17. Russell A.B., Singh P., Brittnacher M.,Bui N.K., Hood R.D., Carl M.A., Agnello D.M., Schwarz S., Goodlett D.R., Vollmer W., Mougous J.D. A widespread bacterial type VI secretion effector superfamily identified using a heuristic approach. *Cell Host Microbe.* 2012; 11(5):538-49.

18. Sandalova T., Lee M., Henriques-Normark B., Hesek D., Mobasherry S., Mellroth P., Achour A. The Crystal Structure of the minor pneumococcal autolysin LytA in complex with a large peptidoglycan fragment reveals the pivotal role of glycans for lytic activity. Accepted article, doi: 10.002/mmi.13435.

19. Schanda P., Triboulet S., Laguri C., Bougault C.M., Ayala I., Callon M., Arthur M., Simore J.P. Atomic model of a cell-wall cross-linking enzyme in complex with an intact bacterial peptidoglycan. *J Am Chem Soc*. 2014; 136(51):17852-60.

20. Shang G., Liu X., Lu D.,Zhang J., Li N., Zhu C., Lui S., Yu Q., Zhang H., Hu J., Cang H., Xu S., Gu L. Structural insight into how Pseudomonas aeruginosa

peptidoglycan hydrolase Tse1 and its immunity protein Tsi1 function. *Biochem. J*. 2012; 448(2):201-11.

21. Silhavy T.J., Kahne D., Walker S. The bacterial cell envelope. *Cold Spring Harb. Perspect. Biol*. 2010; 2(5):a000414.

22. Silverman J.M., Agnello D.M., Zheng H., Andrews B.T., Li M., Catalano C.E., Gonen T., Mougous J.D. Haemolysin coregulated protein is an exported receptor and chaperone of type VI secretion substrates. *Mol. Cell*. 2013; 51(5):584-93.

23. Silverman J.M., Brunet Y.R., Cascales E., Mougous J.D. Structure and regulation of the type VI secretion system. *Annu. Rev. Microbiol*. 2012; 66:453-72.

24. Taneja N., Kaur H. Insights into Newer Antimicrobial Agents Against Gram-negative Bacteria. *Microbiology Insights* 2016; 9: 9–19.

25. Typas A., Banzhaf M., Gross C.A., Vollmer W. From the regulation of peptidoglycan synthesis to bacterial growth and morphology. *Na.t Rev. Microbiol*. 2012; 10(2):123-36.

26. Vivian J.P., Hastings A.F., Duggin I.G., Wake R.G., Wilce M.C.J., Wilce J.A. The impact of single cysteine residue mutations on the replication terminator protein. *Bioch. Biophys. Res. Comm*. 2003; 310(4): 1096-1103.

27. Williamson M.P. Using chemical shift perturbation to characterize ligand binding. *Prog. Nucl. Magn. Reson. Spectrosc.* 2013; 73:1-16.

28. Ziarek J.J., Peterson F.C., Lytle B.L., Volkman B.F. Binding site identification and structure determination of protein-ligand complexes by NMR a semi-automated approach. *Meth. Enzymol.* 2014; 493: 241-75.

Table of Appendices

Appendix 1: Residue assignments for Tae1 in NHSQC, HCACB, CCONH TOCSY, and HCCONH TOCSY Experiments

Protein		NHSQC		HCACB		CCONH					HCCONH								
Res	Num	H	N	CA	CB	CA	CB	CG	CG2	CD	HA	HA2	HB	HB2	HG	HG2	HD	HD2	HE
MET	1	--	--	--	--														
ASP	2	--	--	54.991	41.744	54.474	41.504				4.69		2.72	2.56					
SER	3	8.477	115.399	58.452	64.495	58.107	64.797				4.59875		3.95954						
LEU	4	8.858	126.106	55.583	42.069	55.448	41.801				4.49136		2.88679		1.5647		0.84878		
ASP	5	8.15	114.38	54.174	40.562	54.110	40.286				4.6184		3.00162						
GLN	6	8.023	122.191	60.231	28.186	59.968	28.021	33.984			3.82711		2.10604		2.40331				
CYS	7	8.459	116.846	61.559	35.703	61.659	35.498				4.67705		3.45002	3.0081					
ILE	8	7.464	126.476	64.75	39.048	64.744	38.831	29.150	18.082	13.488	5.37467		3.71812		2.12487	1.72471	0.92207		
VAL	9	8.15	122.258	68.065	32.021	67.806	31.839	23.123	21.776		3.11208		2.03669		1.0394				
ASN	10	8.736	117.342	56.382	37.813	55.880	37.527				4.26073		2.72322						
ALA	11	7.162	121.985	55.287	18.806	54.722	18.597				4.24875		1.45162						
CYS	12	8.211	120.877	64.055	25.658	63.741	25.423				3.68836		2.30153	1.11445					
LYS	13	7.975	119.047	60.233	32.683	59.946	32.426	25.971			3.7635		1.80569		1.32812		1.53205		3.04538
ASN	14	8.207	116.238	55.278	38.816	55.556	38.489				4.53071		2.9785	2.76335					
SER	15	7.878	113.896	61.468	64.107	61.196					4.1722		3.74287	3.52298					
TRP	16	8.017	124.298	61.414	31.464	61.262	31.240				4.45729		3.86148	3.50156					
ASP	17	7.918	111.341	54.733	42.171						4.83736		2.9922	2.61317					
LYS	18	7.125	119.195	56.347	35.608	56.347													
SER	19	--	--	56.648	64.416	56.347					4.54131		3.61572						
TYR	20	8.987	127.628	62.765	39.855		39.625				3.79315		2.40576						
LEU	21	8.07	118.561	52.985	42.906	52.813	42.633	27.008			4.28742		1.55654		1.43385		0.89242		
ALA	22	8.212	126.765	54.476	19.694		17.753				3.89807		1.27652						
GLY	23	8.599	111.624	45.809	--	45.514					4.19563	3.69123							
THR	24	8.33	118.237	59.67	71.438														
PRO	25	--	123.119	63.261	32.963	63.106	32.821	27.855			4.46652		2.27885	2.04241	1.80369		3.80493		
ASN	26	9.156	123.154	55.662	37.701						4.44677		3.35868	2.58078					
LYS	27	7.548	116.213	58.558	30.28						4.73406		1.46687		0.94232	0.67041	0.20659		2.8602
ASP	28	7.289	118.843	53.575	42.746	53.526	42.438				4.90088		2.9686						
ASN	29	7.327	116.395	52.808	40.542	52.659	40.267				4.70873		2.82526	2.56351					
ALA	30	9.119	127.538	56.984	21.329		21.085				4.12611		1.91277						
SER	31	8.582	111.651	61.111	62.67	60.799					4.13514		3.70235						
GLY	32	7.248	111.14	48.169	--						4.19563								
PHE	33	8.342	118.522	63.208	38.556	63.140	38.289				3.98943		3.3406	3.08377					
VAL	34	7.22	116.465	67.556	31.668	67.120					3.06404		1.86513		1.12695				
GLN	35	8.363	118.109	--	--														
SER	36	8.42	118.362	64.025	62.569	64.025							3.85192						
VAL	37	7.613	125.241	67.708	32.121	67.346	31.780				3.05024		1.81217		0.69161	0.29578			
ALA	38	8.284	119.717	55.854	18.53	55.354					3.65339		1.45397						

ALA	39	8.009	119.157	--	18.114		17.852				4.13455		1.5553						
GLU	40	7.852	120.307	59.711	29.289	59.555	29.449	36.325			3.96569		2.06063		2.22128				
LEU	41	7.436	115.601	55.071	43.526	54.723	43.171	28.608			4.21846		1.65782		1.66927		0.78635		
GLY	42	7.912	110.459	46.589	--						3.99067	3.7851							
VAL	43	8.154	124.097	59.7	34.29														
PRO	44	--	--	63.136	31.914	62.937	31.800	27.559			4.27804		2.20319		1.95389		3.49628		
MET	45	7.96	122.777	51.1	35.112														
PRO	46	--	--	63.181	32.639	62.984	32.639	27.197			4.33287		2.32139		1.61525				
ARG	47	8.038	120.031	55.893	32.283	55.668	31.990	27.429		43.484	4.23827		1.70585		1.70585		3.2054		
GLY	48	7.978	106.298	44.357	--	44.256					4.41018	3.65941							
ASN	49	7.848	115.2	51.883	38.12						4.30089		3.54008						
ALA	50	8.398	119.176	56.94	18.544	56.940	18.293												
ASN	51	8.204	116.394	56.1	37.484	56.002	37.291				4.41721		2.81998						
ALA	52	7.862	122.031	55.028	18.479	55.214	18.272				4.12574		1.5155						
MET	53	8.973	120.368	60.215	33.527	59.903					3.43528		1.96741		2.23854				1.69152
VAL	54	8.152	119.353	68.115	31.042	67.893	30.888				3.0813		2.02515		0.96654				
ASP	55	7.668	117.935	58.173	40.475	58.088	40.194				4.31126		2.70982	2.55045					
GLY	56	7.886	106.567	47.359	--	47.069					3.87926	3.40324							
LEU	57	8.586	127.345	58.195	39.162														
GLU	58	--	--	59.312	29.272	59.069	29.272	35.395			4.05312		2.1219		2.34787				
GLN	59	7.176	113.464	57.518	29.847	57.369		33.927			4.30103		2.19481		2.52359				
SER	60	7.695	110.005	60.54	67.061	60.203					4.97129		4.02243						
TRP	61	9.435	126.188	57.291	30.829														
THR	62	8.389	118.896	64.289	70.212	64.093			21.761		4.25978		4.04431		1.12968				
LYS	63	8.683	127.093	55.934	34.252	55.550	33.948				5.12804		1.78238		1.38951		1.38951		2.9802
LEU	64	8.751	124.258	53.362	44.021	53.203	43.723				4.58268		1.55564				0.68609		
ALA	65	8.776	120.673	54.026	20.38		20.119				4.34552		1.45702						
SER	66	7.138	106.868	56.858	66.729						4.83417		4.0317						
GLY	67	8.836	110.291	46.115	--						3.56359	2.70438							
ALA	68	8.118	124.097	55.337	18.211		17.996				3.9992		1.29481						
GLU	69	7.764	119.592	59.336	30.463	59.145	30.651	37.406			3.91654		1.99624		2.23641				
ALA	70	7.498	121.645	55.515	19.588		19.315				3.77275		1.12193						
ALA	71	7.795	119.034	55.464	19.316		19.018												
GLN	72	7.582	117.638	59.099	28.559	58.752	28.704	33.889			4.06773		2.13399		2.39276				
LYS	73	8.198	118.718	57.748	31.056	57.527	30.853				4.11905		1.9299		1.42129		1.16373		2.45428
ALA	74	8.247	125.013	55.55	17.988		17.729				5.05448		1.45125						
ALA	75	7.904	117.944	54.747	18.507	54.649	18.262				4.15769		1.66571						
GLN	76	7.59	116.341	56.002	29.693	55.807	29.015	34.266			4.39819		2.50602		2.7154				
GLY	77	8.277	106.739	46.292	--	46.194					4.10221	3.50777							
PHE	78	7.801	118.747	57.862	41.505	57.417	41.246				4.722		2.66342						
LEU	79	9.745	123.944	55.224	42.117	54.927	41.847				4.61736		2.13382		1.71498		1.12089	0.94393	
VAL	80	9.822	129.925	60.731	34.566	60.488	34.356				5.4048		2.16219		1.03043				

ILE	81	9.6	126.565	56.788	40.088	56.526	39.740	28.128	17.237		5.36585		1.94094		1.68937	1.04515	0.78128		
ALA	82	9.249	129.236	49.527	21.847		21.595				5.4477		1.23719						
GLY	83	9.006	106.733	46.53	--	46.413													
LEU	84	8.137	122.212	55.743	46.268	55.626	46.113				4.57225		1.79818		1.25307		0.88434	0.7021	
LYS	85	9.105	130.354	58.366	33.184	58.131	32.931	26.126			4.64234		1.63949		1.40487		1.05385		2.76264
GLY	86	8.688	108.723	43.835	--														
ARG	87	8.07477	131.638	--	--						4.3509		1.73781				3.24883		
THR	88	--	--	--	--														
TYR	89	--	--	57.031	40.832	57.195	40.593				4.86314		3.31133	3.06416					
GLY	90	8.674	111.011	44.754	--	44.666					4.50977	3.87196							
HIS	91	8.06	115.87	57.748	33.577		33.299				4.87675		2.9214						
VAL	92	5.791	115.395	58.546	37.656	58.216	37.381				5.73063		1.90775		0.86316	0.66108			
ALA	93	9.267	121.566	51.427	24.519	50.548	24.239				4.85868		1.35962						
VAL	94	9.358	122.332	62.863	34.449	62.616	34.136				4.69736		2.37228		1.08082	0.89695			
VAL	95	9.018	129.916	63.529	32.489	63.257	32.360				4.48127		1.99259		1.18665	0.98276			
ILE	96	7.787	117.645	59.294	41.46	59.092	41.357				4.88934		2.21985		1.44531	1.0209	0.75009		
SER	97	8.71	114.369	59.112	64.491	58.764					4.33343		3.95279	3.74295					
GLY	98	7.874	109.356	44.589	--														
PRO	99	--	--	63.198	32.338		32.085	27.386			4.2756		2.25379		1.89207		3.59609		
LEU	100	8.094	118.082	54.213	42.102	54.004	41.763				4.1586		1.6435		1.39482		0.58535		
TYR	101	9.197	129.032	58.404	39.137		38.884												
ARG	102	--	--	57.129	--	57.063				43.292	3.67045		1.95628	1.59009	0.69057		2.91785		
GLN	103	7.774	106.98	58.821	27.446						3.61535		2.27979						
LYS	104	7.327	116.413	--	--														
TYR	105	--	--	--	--														
PRO	106	--	--	63.178	34.414	62.911	34.240	27.941			4.67818		2.1568		1.96814		2.50043		
MET	107	9.417	120.069	54.741	30.659	54.411					4.68092		1.81988		2.76585				
CYS	108	8.052	110.77	56.83	34.421	56.605	34.156				6.26065		2.87336						
TRP	109	9.61	120.696	57.11	34.203	56.871	33.886				5.03618		3.60476	3.33425					
CYS	110	9.415	113.804	56.993	30.946		30.677				5.12075		3.41935						
GLY	111	7.737	107.733	43.575	--	43.146					4.4355	3.55262							
SER	112	8.205	107.524	59.863	65.268						4.49356		4.07778	3.24877					
ILE	113	8.955	133.45	62.513	38.58	62.351	38.302	28.938	16.218	14.162	4.14994		1.85346		1.45267	1.18735	0.75376	0.54783	
ALA	114	8.409	124.196	52.778	18.948		18.677				4.10093		1.16481						
GLY	115	7.413	105.563	44.355	--	44.223					4.25446	3.66678							
ALA	116	8.496	124.61	55.923	18.745	56.119	18.535				3.93664		1.39756						
VAL	117	7.918	112.732	64.609	31.678	64.376	31.410				3.81068		2.02281		0.81251				
GLY	118	7.562	107.192	44.571	--	44.506					4.10107	3.28174							
GLN	119	6.977	117.521	54.728	31.268	54.422		33.613			4.34257		2.14151		2.74711				
SER	120	8.866	112.118	57.261	65.003	57.008					4.40856		3.16622						
GLN	121	8.48	131.034	52.175	28.089	52.100		33.269			2.69445		-0.00026		0.81986				
GLY	122	5.981	104.739	45.651	--						3.54682	3.01138							

LEU	123	6.272	114.225	54.721	43.353		42.968				3.81711		1.56007		1.20945		0.70934		
LYS	124	7.581	117.832	54.316	--	54.316					4.49136		1.5647		1.19173				
SER	125	8.151	113.669	56.799	67.693		67.349				4.10652		3.61312						
VAL	126	9.397	117.672	65.012	31.237	64.760	31.089				4.51251		2.80803		1.30241	1.46771			
GLY	127	7.96	103.673	45.842	--	45.580					3.78418	2.72885							
GLN	128	7.485	116.226	56.462	32.455	56.190		35.090			4.43083		1.79036	1.25345	2.22798				
VAL	129	7.106	114.632	64.113	32.78	63.783	32.631				3.94528		1.88867		0.77523	0.42237			
TRP	130	7.375	119.77	59.913	31.222		31.070				4.6289		3.15939	2.94091					
ASN	131	9.094	116.291	52.336	38.688														
ARG	132	--	--	59.647	30.485	59.647	30.485				3.69882		1.85689		1.64613		3.21803		
THR	133	7.879	113.89	64.751	69.186	64.384			21.923		4.20772				1.20095				
ASP	134	8.595	123.629	57.154	41.066						4.28281		2.56388						
ARG	135	8.505	114.648	58.693	29.274	58.434	29.223				3.64535		1.83315		1.46152		2.64322		
ASP	136	7.182	117.118	55.297	41.449						5.24888		3.12372	2.53614					
ARG	137	7.885	119.436	55.311	31.028	55.098				43.765	4.56841		1.89373		1.64485		3.22938		
LEU	138	6.234	115.501	55.605	42.805	55.288	42.552				3.38678		1.07475		0.18509		-1.07008		
ASN	139	7.068	116.088	51.739	43.582						4.68121		2.60922	1.74593					
TYR	140	8.645	119.17	56.923	41.79	56.565	41.515				5.05283		2.59112	2.39688					
TYR	141	9.452	123.016	56.79	42.347	56.672	42.139				5.55639		3.22528	2.78493					
VAL	142	9.492	122.153	58.914	36.505	58.719	36.242				5.72828		1.79202		1.06855	0.79661			
TYR	143	7.816	129.667	58.023	37.387						5.35775		3.31256						
SER	144	8.397	118.6	--	63.451						3.88587		3.51897						
LEU	145	6.377	120.425	53.739	45.673						4.58963		1.46184		0.8526				
ALA	146	8.36	125.723	53.263	17.813		17.534				3.06241		0.61941						
SER	147	8.403	119.781	61.406	65.568	61.180					4.57994		3.89997	3.49345					
CYS	148	7.931	118.222	52.872	38.352	52.821	38.154				5.06153		3.76573	3.14869					
SER	149	8.352	115.443	57.906	65.347	57.468					4.51948		3.76201						
LEU	150	8.283	124.408	53.553	42.246														
PRO	151	--	--	63.465	--	63.212				50.764	4.4233		2.28373		1.94249		3.87214	3.64175	
ARG	152	8.394	121.773	56.285	31.299						4.30108		1.85722	1.65319	1.39821		3.21038		
ALA	153	8.003	131.465	--	--						4.36314		1.40854						
SER	154	7.929	121.011	--	--														
LEU	155	--	--	--	--														
GLU	156	--	--	--	--														
HIS	157	--	--	--	--														
HIS	158	--	--	--	--														
HIS	159	--	--	--	--														
HIS	160	--	--	--	--														
HIS	161	--	--	--	--														
HIS	162	--	--	--	--														

Appendix 2: Residue Assignment for Tae1 in HCCH COSY and HCCH TOCSY Experiments

		HCCH COSY Assignments										HCCH TOCSY Assignments									
Residue #		Ha1	Ha2	Hb1	Hb2	Hg1	Hg2	HCD1	HCD2	HCE1	HCE2	Ha1	Ha2	Hb1	Hb2	Hg1	Hg2	HCD1	HCD2	HCE1	HCE2
1	met																				
2	asp	4.563			2.640							4.714		2.747	2.569						
3	ser	4.577			3.956							4.579		3.953							
4	leu	3.367			-0.227	0.943		-0.041	-0.036			3.367		0.757		0.957		-0.039	-0.039		
5	asp	3.620		2.267								4.604		3.300	3.073						
6	gln	3.838		2.340		2.350						3.826		2.041		2.425					
7	cys	4.660		3.442	3.003							3.642		2.263							
8	ile	3.762		2.110		1.116	0.928					3.743		2.132		1.108	0.935				
9	val	3.115		2.026		1.059						3.104		2.035		1.053					
10	asn	4.281		2.734																	
11	ala	3.903		1.316								3.896		1.270							
12	cys																				
13	lys	4.307		0.958		0.917		1.418		2.885		4.298		0.888	0.216	0.853		1.420		2.885	
14	asn	4.555		2.995	2.782							4.538		2.978		2.759					
15	ser	4.445		3.852								4.463		3.846							
16	trp																				
17	asp	4.854		3.106	2.652							4.866		2.993	2.624						
18	lys	3.749		1.805		1.536		1.718		2.989		3.745		1.816		1.536		1.722		3.033	
19	ser	4.546			3.628							4.541		3.612							
20	tyr	3.846		2.426								3.813		2.444							
21	leu							0.310										0.310			
22	ala	3.889		1.275								3.888		1.270							
23	gly	4.177	3.686									4.200	3.682								
24	thr																				
25	pro																				
26	asn	4.412		2.811								4.419		2.814							
27	lys																				
28	asp	4.949										4.913									
29	asn	5.054		3.768	3.177							5.055		3.708	3.144						
30	cys30***ala***											4.250		3.177							
31	ser	4.965		4.077								4.940		4.077							
32	gly											3.702	3.545								
33	phe	4.672		2.326								4.660		2.442							
34	val																				
35	gln																				
36	ser	4.129			3.841							4.151		3.845							
37	val	3.060*		1.818		0.083						3.093		1.807		0.721					

38	ala	3.942		1.394								3.945		1.394							
39	ala	4.124		1.542								4.119		1.540							
40	glu	4.038			2.150	2.618?	2.572?					3.960		2.252	1.993	2.112	2.097				
41	leu	4.330		1.505		1.513		0.689				4.332		1.478		1.193		0.703			
42	gly											3.989	3.743								
43	val	3.952		1.503		0.168						3.935		1.499		0.168	0.168				
44	pro	4.4175		2.278	1.8851	2.0113		3.846	3.6388			4.4806		2.2833		2.0288		3.8486			
45	met											5.257		1.872	1.657	1.872	1.667				
46	pro	4.3288		2.278	1.6326	1.6369		3.6171	3.4745			4.2554		2.2929		1.7237		3.6222			
47	arg	4.230		1.679		1.649		3.193				4.236		1.747		1.678		3.198			
48	gly	4.383	3.629									4.241	3.661								
49	asn													2.723							
50	ala	4.235		1.669								4.240		1.653							
51	asn											4.262		2.714							
52	ala	4.134		1.505								4.341		1.443							
53	met	3.434		1.955	1.666	2.245	2.010					3.441		1.999	1.697	2.048	1.886				
54	val	3.1929*		2.009								3.078		2.015		0.819					
55	asp	4.611		3.043								4.310		2.708	2.541						
56	gly	3.893	3.387									3.866	3.402								
57	leu					1.661		0.689													
58	glu	3.9185		1.9856		2.2586						3.9328		1.9867		2.3029	2.1686				
59	gln	4.292		2.189	2.196	2.5341*	2.5341*					4.285		2.246	2.139	2.522					
60	ser											4.228		3.828							
61	trp											4.070		2.458	2.347						
62	thr	4.276		4.057		1.149						4.261		4.057		1.125					
63	lys	5.100		1.780		1.379						5.112	1.775		1.353		1.780		3.030		
64	leu											4.575		1.567		0.668		0.753	0.753		
65	ala	4.344		1.469								4.340		1.452							
66	ser																				
67	gly	3.583	2.693									3.573	2.680								
68	ala	4.649		1.668								4.560		1.645							
69	glu	3.967		1.790		1.831						3.964		1.384		1.812					
70	ala	3.787		1.566								3.812		1.558							
71	ala	3.770		1.117								3.779		1.112							
72	gln																				
73	lys	4.127		1.950		1.441	1.100	1.439	0.932	2.488	2.173	4.121		1.937	1.407	1.483	1.622	1.408	0.949	2.485	2.175
74	ala	3.997		1.2822								3.967		1.268							
75	ala	4.178		1.664								4.164		1.657							
76	gln	4.371		2.018	2.043	2.348						4.314									
77	gly		3.481									4.084	3.498								
78	phe	4.872		2.971								4.867		2.950							
79	leu	4.284		1.573		1.498		0.839				4.294		1.570		1.480		0.928	0.925		

80	val			2.286		0.953								2.337		1.073					
81	ile	5.367		1.931		1.688	0.753	0.771				5.362		1.915		1.670	0.768	0.781			
82	ala																				
83	gly	5.334	3.701									5.359	3.655								
84	leu	4.548				1.795		0.839				4.578		1.805		1.757		0.836	0.836		
85	lys																				
86	gly	4.582	3.681									4.589	3.730								
87	arg	3.980		1.831		1.630															
88	thr	4.217		3.920								4.215		3.957		0.994					
89	tyr																				
90	gly	4.380	3.718									4.589	3.934								
91	his											4.383		3.929							
92	val	5.7548		1.9246		0.8389						5.7259		1.89		0.8656	0.8656				
93	ala																				
94	val	4.088		2.017		0.845						4.058		2.023							
95	val	3.965		2.026		0.836															
96	ile	4.897		2.124		1.405		1.104				4.885		2.219		1.470		1.105			
97	ser	4.389			3.845							4.397		3.850							
98	gly	4.136	3.300									4.451									
99	pro	4.4175		2.2781	1.8885	2.0164		3.6027				4.2559		2.2747		2.1239		3.6207			
100	leu											4.176		1.396		0.608		0.463	0.463		
101	tyr											4.588		3.957							
102	arg																				
103	gln	4.657		1.398		1.382						4.649		1.658		1.445					
104	lys	4.307		0.669		0.737		1.661		2.885		4.291		0.796	0.662	0.974	0.756	1.412	1.422	2.882	2.733
105	tyr	4.262		2.679								4.221		2.727							
106	pro																				
107	met											4.035		2.093		2.500					
108	cys	4.448		3.175	3.175							4.398		2.720	2.502						
109	trp	4.564		2.979								4.552		2.999							
110	cys											4.566		3.178	3.041						
111	gly	4.427	3.497									4.441	3.557								
112	ser	4.581			3.808							4.397		3.857							
113	ile	4.129		1.831		1.423		0.783				4.141		1.865		1.185	1.416	0.794			0.777
114	ala	4.104		1.163										1.610							
115	gly	4.415	3.660									4.410	3.664								
116	ala	4.217		1.439								4.251		1.465							
117	val	3.797		1.993		0.838						3.816		2.024		0.780					
118	gly	4.415	3.730									4.097	3.284								
119	gln	4.728										4.033		2.601		2.124					
120	ser	4.495			3.783							4.517		3.757							
121	gln	3.807		2.026		2.378						3.793		1.793		2.303					

122	gly																				
123	leu	4.3409		1.3647		1.2076		0.7288				4.322		1.4941		1.1999		0.7278			
124	lys																				
125	ser	5.320			4.089							5.321		4.117							
126	val																				
127	gly	4.195	3.672									3.523	3.002								
128	gln																				
129	val	3.937		1.857		0.732						3.963		1.882		0.431	0.821				
130	trp											4.504		3.008							
131	asn	4.417		3.392	2.840							4.406		3.422							
132	arg	3.702		1.846		1.617		3.193				3.705		1.853	1.848	1.564		3.202			
133	thr	4.255		4.169								4.223		3.934		1.199					
134	asp	4.255		2.605								4.282		2.666	2.562						
135	arg																				
136	asp	4.485		1.520								4.227		3.199							
137	arg	4.612			3.141																
138	leu	3.3957		1.0169		0.1513		-1.042				3.3847		1.1137		0.1607		-1.081			
139	asn																				
140	tyr																				
141	tyr																				
142	val																				
143	tyr	4.157		2.169								4.162		2.149							
144	ser																				
145	leu																				
146	ala																				
147	ser											4.566		3.963							
148	cys			2.998	2.754							2.976		2.748							
149	ser	4.384		3.852								4.396		3.853							
150	leu																				
151	pro																				
152	arg																				
153	ala	4.286		1.379																	
154	ser	4.393			3.845																

Appendix 3: NHSQC Experiment with Assignments Shown

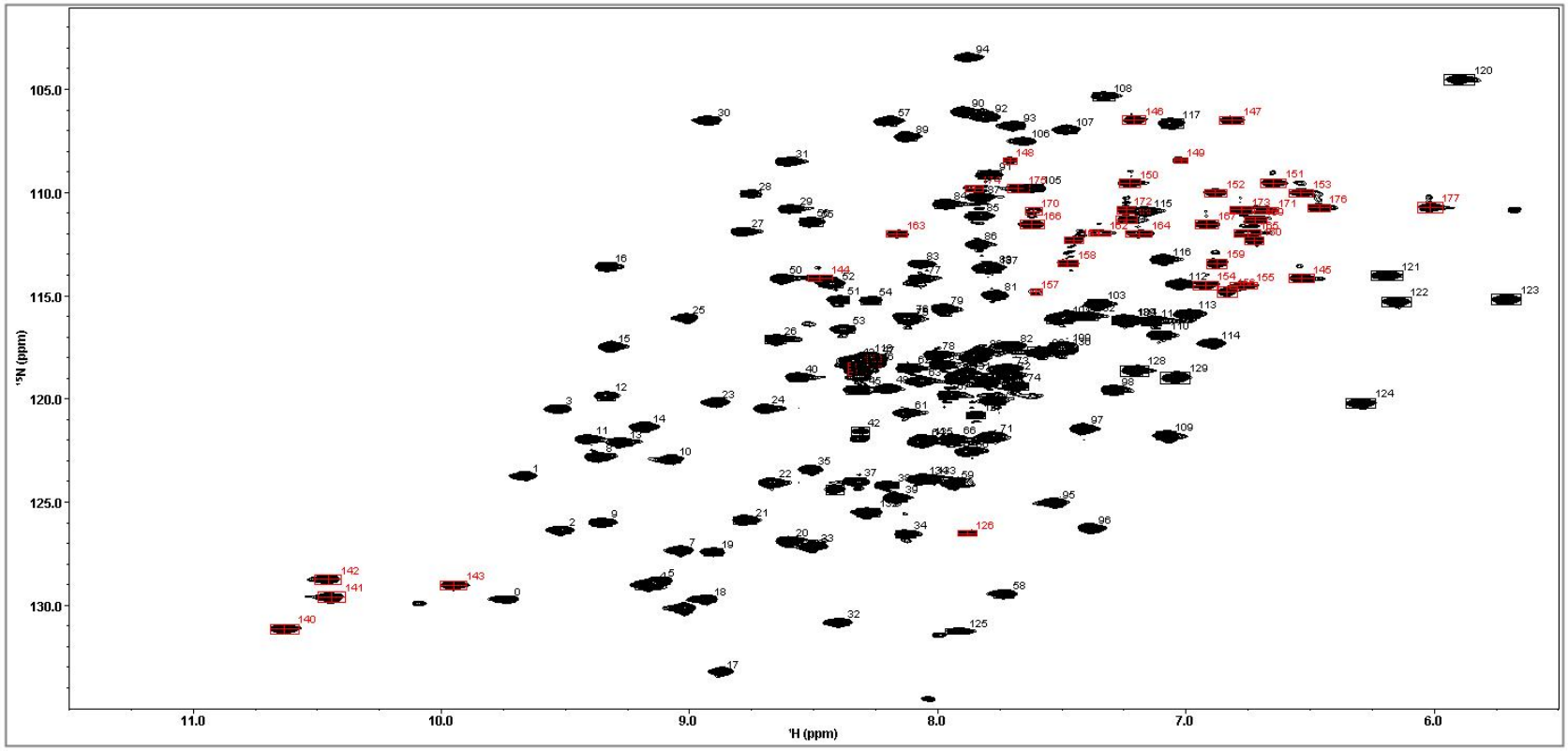

Appendix 4: CHSQC Experiments with assignments shown

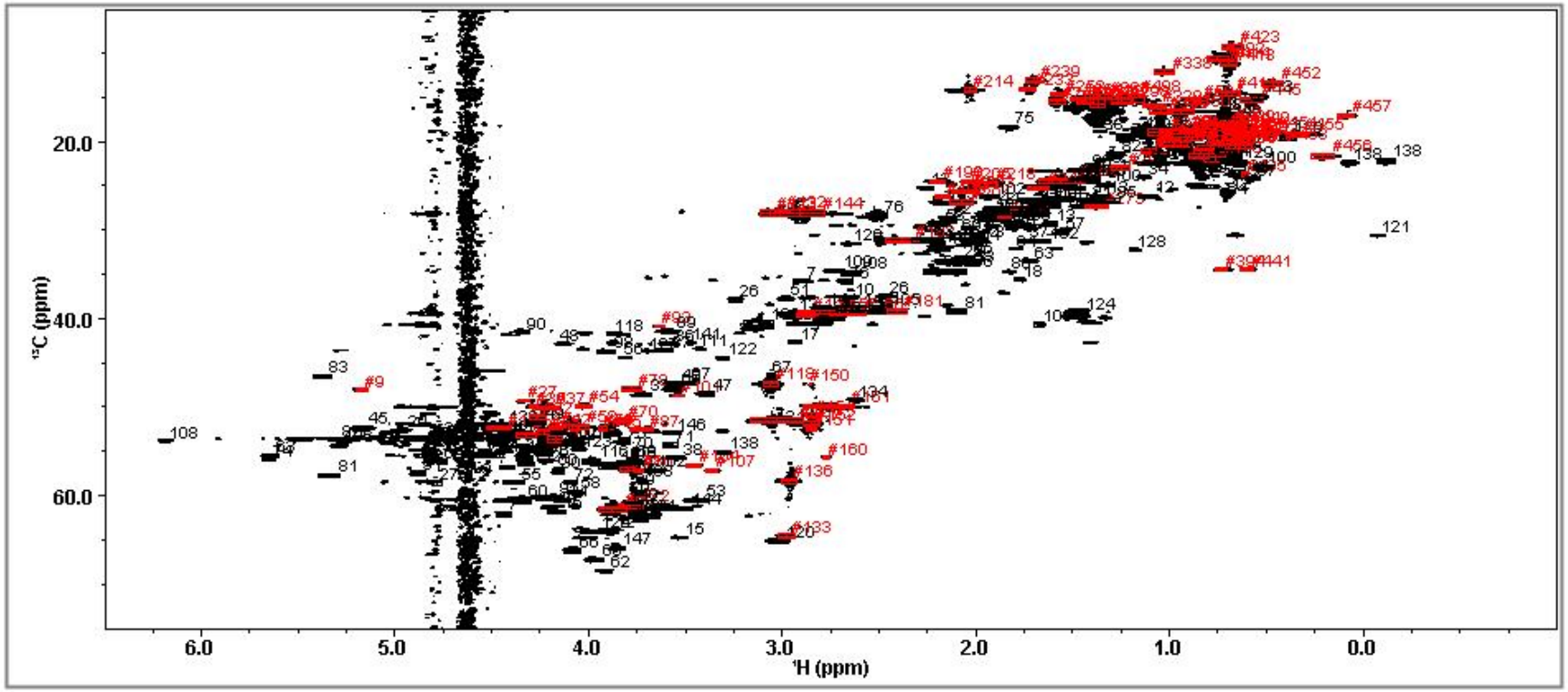

Appendix 5: Graphical Comparison of NMR (NHSQC) peak intensity of WT-Tae1 Titration with Hcp1

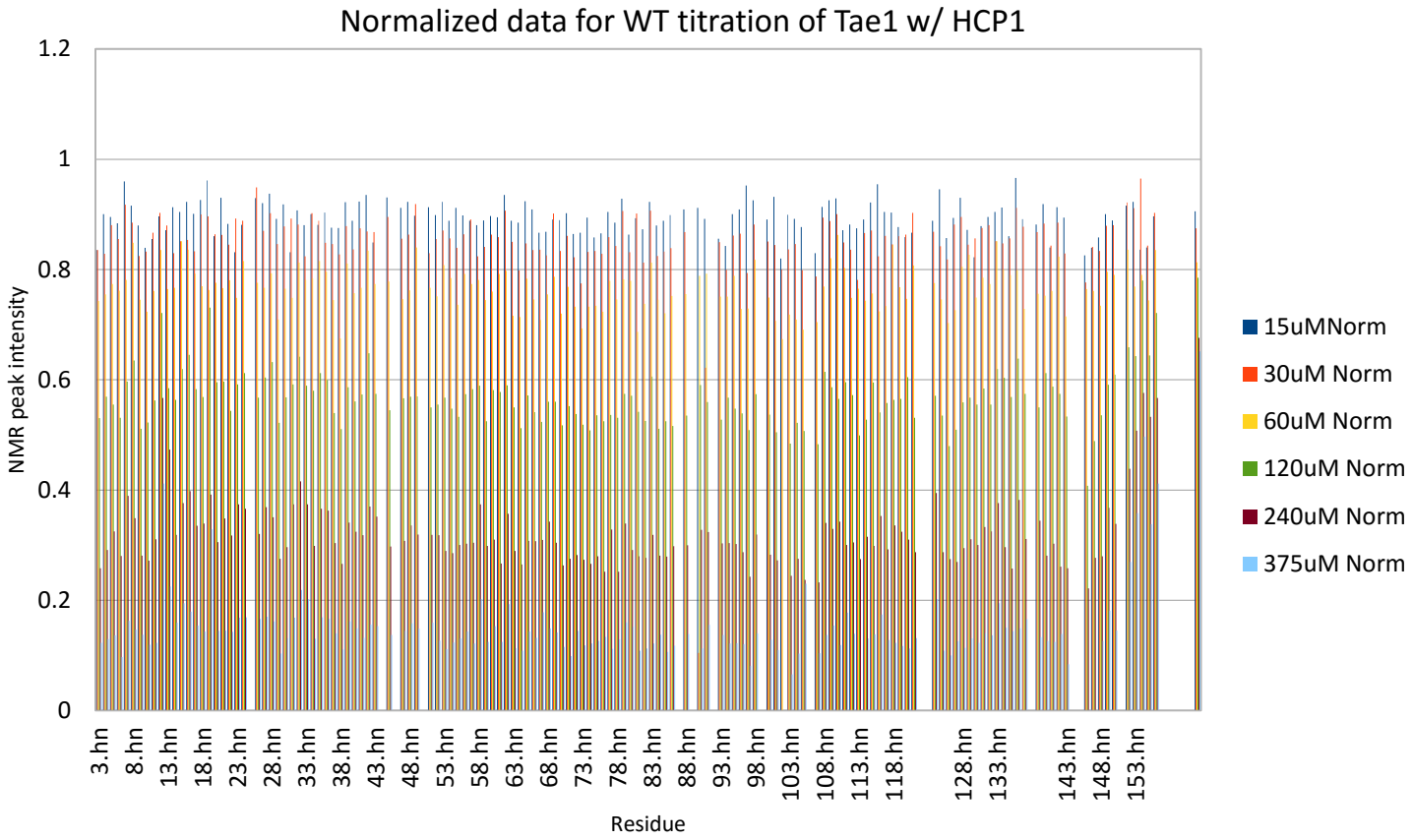

Appendix 6: Graphical Comparison of NMR (NHSQC) peak intensity of Tae1-S115Q Titration with Hcp1

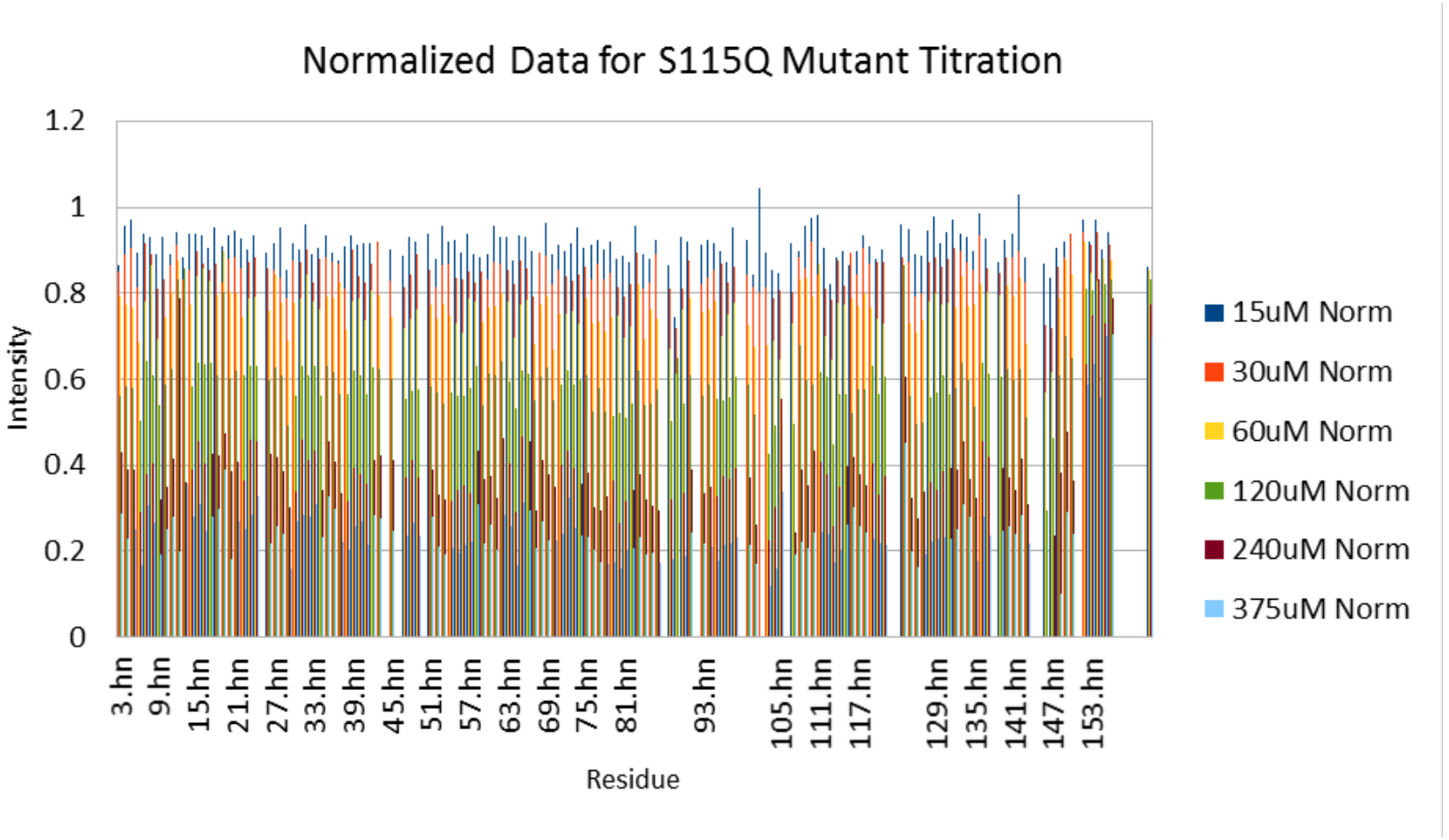

Appendix 7: Experimental Design for Confirmation of Tae1 Minimal Binding Fragment Specificity